



Eidgenössische Technische Hochschule Zürich
Swiss Federal Institute of Technology Zurich

Nighttime lights as proxy for the spatial growth of dense urbanized areas

Master Thesis

Nicola Pestalozzi

Supervisor: Prof. Dr. Didier Sornette
Tutors: Dr. Peter Cauwels
Monika Niederhuber

ETH Zürich
Department of Management, Technology and Economics (D-MTEC)
Chair of Entrepreneurial Risks
Chair of Land Use Engineering

November 2012

Abstract

Nighttime lights constitute a very appealing database that can be used to measure various different aspects of the human footprint on the planet. The amount of research and the number of publications around this dataset confirm this, offering a broad spectrum of applications that involve economics, energy, society and environment.

I chose to use them to study the spatial extension and the relative distribution of settlements around the Earth and their evolution over time. I analyzed the DMSP-OLS 'stable lights' database of the NGCD consisting in a catalog of world images of the last 19 years.

I discovered that the mean center of lights is moving steadily to South-East. This reflects the extreme growth experienced by the urban centers in the developing countries, especially in Asia. I further developed a version of the Gini coefficient to compare the statistical spatial dispersion of nighttime lights, unexpectedly finding that all the countries show a very similar inequality value, quickly converging to the same coefficient by raising the lower threshold of light detection.

Further, I analyzed the evolution of the lit area at a country level and in the largest urban agglomerations, finding that whereas most developing countries and cities are experiencing an incredible spatial growth in illumination, some 'historical' conurbations present rather constant or even decreasing emissions. This could be a signal of success of the light pollution abatement programs launched in the last years.

Acknowledgments

I wish to heartily thank the whole Land Use Engineering Research Group (LUE) of Professor Hans Rudolf Heinimann and especially Monika Niederhuber for the helpfulness demonstrated to me from the beginning, both on the administrative and the technical sides. I could profit from an excellent infrastructure and the deep know-how of different people, especially in the field of ArcGIS, which was completely new to me (a special thank goes here to Daniel Trüssel for its expertise, helpfulness and especially patience). At least as much important as that, I could work in a really pleasant environment, with extraordinary people that made me feel part of a team: Maja Messerli, Sarah Brugger, Daniel Mandallaz, Jochen Breschan, Leo Bont, Fabian Gemperle, Franziska Baumgartner and Andreas Hill.

A big thank you goes to Professor Didier Sornette and Peter Cauwels for tutoring my thesis. They provided me many useful inputs and comments during our frequent meetings and they supported me during the whole project, also together with other researcher from the Chair of Entrepreneurial Risks.

Thanks also to Luc Girardin and Sebastian Schutte from the International Conflict Research Group (ICR) of Professor Lars-Erik Cedermann for their help, especially in the initial phase of the thesis.

A special thanks goes finally to all my friends and relatives that supported me directly or indirectly during the writing of the thesis: you are for me the best thinkable motivation.

Website

In order to present the results of this research, I built a website which integrates the full thesis text, color figures, a Poster in format Ao and several animations of the nighttime lights evolution over the years for some interesting regions of the world.

The structure of the website follows the sections of the thesis, even if some modifications were made to fit the content in the web-layout.

The Website is permanently stored in the ETH Web-Archive under the following URL:

<http://www.worldatnight.ethz.ch>

For any comment or additional information about the thesis and the website, please contact me at the following email address: nicola.pestalozzi@gmail.com.

Table of Contents

Abstract	i
Acknowledgments	iii
Website	v
Table of Contents	vii
1 Introduction	1
2 Nighttime lights	3
2.1 Motivation	3
2.2 Data source	4
2.3 The products	5
3 Past research	11
3.1 Economic activity	11
3.2 Population estimation	12
3.3 Power consumption and distribution	13
3.4 Poverty and development index	13
3.5 Effects of wars	14
3.6 Urban extent	15
3.7 Environmental issues	16
3.8 Evaluation Table	20
4 Preprocessing	23
4.1 Software	23
4.2 Product choice	24
4.3 Gas flares removal	25
4.4 Intercalibration	26
4.5 Reprojection	30
4.6 Average satellite/year	31
5 Mean center of lights	33
5.1 Motivation	33
5.2 Method	34
5.3 Results	35
6 Spatial light Gini	37
6.1 Motivation	37
6.2 Methods	37
6.3 Results	40
6.4 Evolution over time	43
6.5 Related research and distinctions	46
7 Urban growth	47
7.1 Motivation	47
7.2 Methods	47
7.3 Results	47
7.4 Agglomeration size	53
8 Conclusions	57
8.1 Main findings	57
8.2 Selected findings from the existing literature	58
8.3 Directions for future research	59
9 List of abbreviations	61
10 List of Figures and tables	63
11 References	65

1 Introduction

The first time I was confronted with a satellite image of the world at night was quite long ago: precisely the 27 November 2000. I just started the high school and since I was very excited about science in general, I checked quite often a website that my astrophysicist brother earlier suggested to me, called APOD¹. APOD stands for Astronomy Picture Of the Day, it is a website hosted by the NASA and, as the name suggests, it publishes every day a picture of an astronomy-related subject. Most of the time it features stars, galaxies or planets far away from us, viewed from telescopes or satellites and colored in the post-processing in order to obtain a pleasant optical effect. Sometimes there are also scientific charts or great pictures of infrastructures like space shuttles, space probes or rovers.

That day there was a picture called "Earth at Night" which shows a map of the nighttime lights worldwide (Figure 1.1) .The effect is astonishing since even without any border or geographical reference², everyone can at a glance easily recognize the shape of the continents, some countries and the major cities. It also gives a feeling of which areas of the world are more developed or densely populated, and how human settlements are spatially organized. It doesn't wonder that this picture has become a famous poster that hangs on many walls³.



Figure 1.1 - Nighttime lights of the world. Source: APOD¹

Almost twelve years later, when it came to decide a topic for my master thesis, I stumbled upon a project proposal from Prof. Sornette about the nighttime lights. I immediately remembered the stunning image seen long before and I was attracted by the possibility to use the data for a scientific research. So I started to investigate which

¹ <http://apod.nasa.gov/apod/>, or for the specific picture: <http://apod.nasa.gov/apod/ap001127.html>

² Actually, some filters and shadings were applied here to better distinguish the continents from the oceans

³ Among others, the one of my tutor's office

data were available and how they could be used, discovering a huge research field with a lot of publications and many different usages of the data.

In chapter 2 I give an extensive motivation of why nighttime lights are an interesting measure and which features makes them different from other land cover data. Further I describe how they are captured and which kinds of product are available.

In the subsequent chapter I then scrutinize the past literature in order to understand which applications have already been developed, starting from which product and with which methods. This is a major component of this research, since the field was completely new to me. I finally tried to judge the quality of the publications by analyzing the level of accuracy with which the data was processed.

Chapter 4 describes my choices of the software, the sources of data, and all the preprocessing steps that I performed on the data before doing my analyses. The reason for these preliminary computations is also explained. I tried to carefully document every step in order to give the possibility to reproduce my results and possibly build further studies upon them.

In the fifth chapter I present the concept of *mean center of lights*, which is a nighttime light based center of gravity of the planet. It builds upon a recent study on the global GDP center of gravity from McKinsey, confirming the finding that the trend of the last decades shows a clear shift toward South-East.

Chapter 6 introduces the formulation of a *spatial light Gini coefficient*, a measure of the relative dispersion of light in space. I computed this indicator per every country and I unexpectedly found a very interesting coincidence of the values. The ratio between the amount of bright and dim lights seems to follow a common pattern throughout the world. The evolution over time shows further a weak trend toward more inequality in the light distribution.

In the last chapter I evaluate the size and the evolution of the urban areas per country and per agglomeration. Some developed countries show a general decline in bright light emissions over the last two decades, whereas the developing countries experienced an incredible growth of lit area. This trend is very well observable at both national and regional scale.

In the conclusions I first summarize my main findings; then I present selected findings from the existing literature and finally suggest some possible directions for future research with this dataset.

2 Nighttime lights

2.1 Motivation

Why use nighttime lights *anyway*? What is so special about them and which features make them more convenient, if at all, in respect to other datasets?

First of all, light emission is an objectively and systematically measurable quantity. This should not be underestimated since we cannot say the same of many other widely used indicators: gross domestic product, energy consumption, population count and density, poverty level and many other economic and demographic indicators are based on estimates, assessments and approximations, which are only partially reliable: they are often collected from different organizations, in different countries, different timeframes, with different methods and at different granularities. Biases and inaccuracies are therefore unavoidable and the comparison of these variables between different countries is always problematic. On the contrary, nighttime lights are remotely sensed from one single satellite, with the same resolution, at the same time and in the same way for the whole world¹, thus delivering a more objective and independent measurement.

The measures captured in satellite imagery are obviously also geographically specific, i.e. they corresponds to a well-defined region of the earth, with a resolution up to few meters. This is not the case for most country statistics, which lack potentially significant geographical and spatial information. Consequently, remote sensing is definitely a more accurate way of measuring the world, but why nighttime lights and no other variables, like for example land cover data? The answer is quite straightforward and relies on the nature itself of lights on earth: they are unquestionably human-made. As we will see, there are some exceptions, like big forest fires, lightning and moon light reflections, but these are mostly ephemeral events that can be recognized and filtered out. If we look at lights that are stable, i.e. observable virtually every night for several hours, then we are almost certainly looking at human-made light. This is a huge advantage over other measures of land cover, since during day and with normal satellite pictures, it is not always that easy to distinguish between man-made and natural structures.

Yet another reason to use nighttime lights is that the gathering of the data is relatively cheap. Although the initial investment can be considerable, the measurements are then collected very quickly and at a fairly high resolution, so that they can be assessed far more often than other traditional indicators.

¹ We will see later that this is not completely true, but for the sake of comparison it can be said that satellite-based observations are in general way more objective than human collected statistics.

2.2 Data source

The database I considered in this research comes from the US Air Force Defense Meteorological Satellite Program (DMSP), and it is archived at the National Geophysical Data Center (NGDC) of the National Oceanic and Atmospheric Administration (NOAA).

The DMSP mission started in the mid-1960's under the control of the Department of Defense (DoD), in order to provide the military with information about the cloud cover worldwide on a daily basis. Scrutinizing the results, it was discovered that the nighttime lights were also very well captured by the sensors. This unexpected but very convenient side-effect gained more and more relevance among the scientific community, and now the NGDC has a research project dedicated exclusively on developing scientific products and applications of this dataset.

The system was declassified in 1972 and made publicly available. Since 1992, the products were digitized and are now downloadable for free from the web.

2.2.1 The satellites

The DMSP Satellites of the actual series (Block-5D) fly in a sun-synchronous low earth orbit (833 km mean altitude) such that they pass over any given point on earth between 20:30 and 21:30 local time (Elvidge, et al., 2001). With 14 orbits per day, each DMSP satellite provides global night-time coverage every 24 hours. There are normally 2 satellites orbiting simultaneously and each satellite has a lifespan of 6 to 8 years (see table 2.1 in section 2.3 for an overview of the satellites used over the years).



Figure 2.1 - Visualization of a DMSP Satellite. Source (United States Strategic Command, 2001)

2.2.2 The sensors

The sensor arrangement is called Operational Linescan System (OLS) and consists in two broadband sensors, one for the visible/near infrared (400 to 1100 nm) and one in the thermal/infrared wavelength (10.5-12.6 μm). The OLS is an oscillating scan radiometer with a field of view of about 3'000 km and captures images at a resolution of 0.56 km, which are then smoothed on-board into 5x5 pixels in order to reduce the memory usage (Doll, 2008).

2.3 The products

Creating good-quality global images from the sub-orbital data of the satellites is an undertaking of monumental difficulty and requires a huge processing effort. Figure 2.2 gives an idea of what a satellite swath looks like before any post-processing. In fact, only a small portion of the data is usable because some parts of the images capture already the daytime light. Further, the areas with a scan angle greater than a certain threshold have to be excluded because, at the edge of the swath, the OLS suffers from poor geolocation accuracy and background noise (Baugh, et al., 2010).

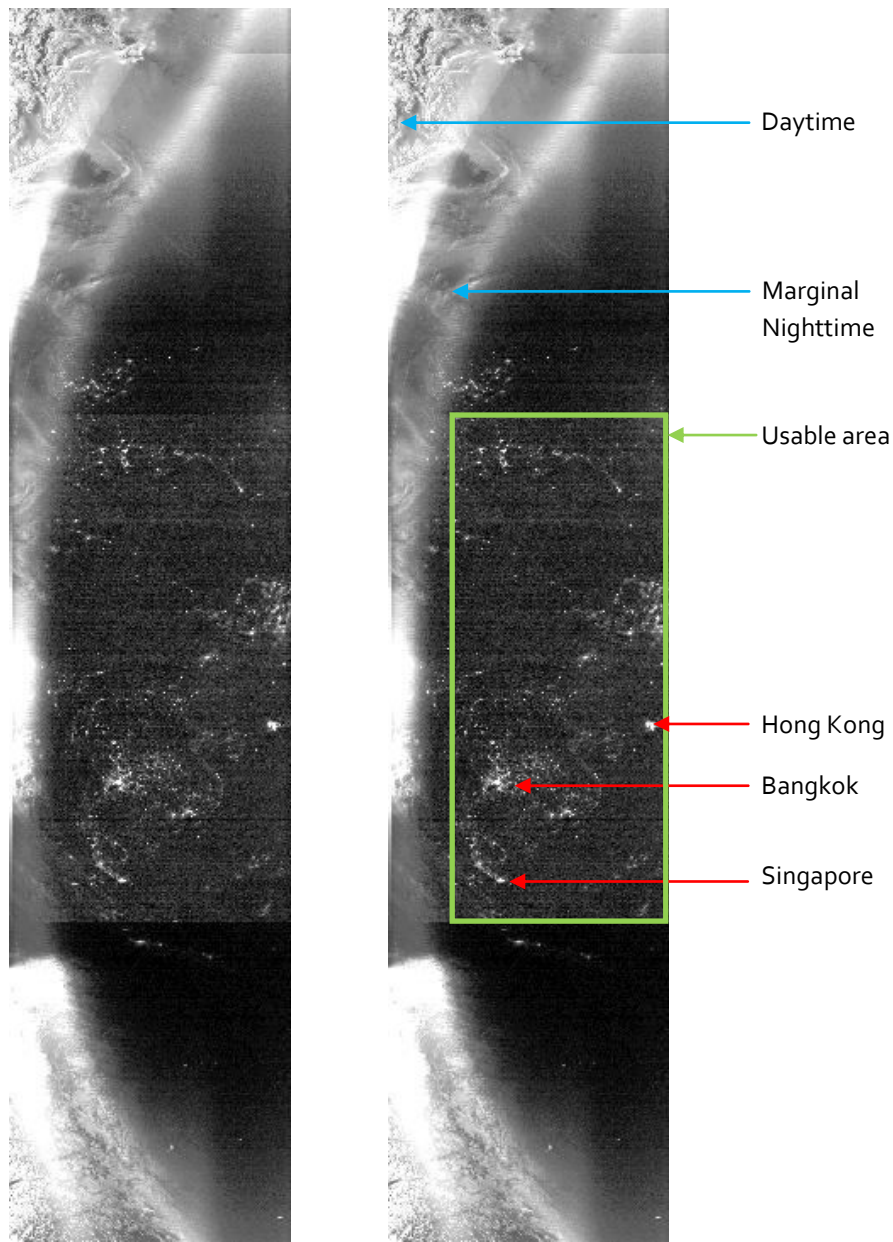


Figure 2.2 – Original portion of an orbit of the satellite F16 over Asia in 2009 (source: (Baugh, et al., 2010)) and relative description of the observable features.

The images were then re-projected into 30 arc-second grids. The geolocation, i.e. the assignation of latitudes and longitudes to each OLS pixel, was made by the NGDC based on different variables such as scan angles, satellite altitude, azimuth etc.

All the satellite sub-orbits were then interleaved to obtain a global composite that covers the whole world. Since many observations were disturbed by clouds, moonlight, sun glare and other factors, the composites have a timeframe of a year, i.e. every image represents the average of one year of observations. In the typical annual cloud-free composite most areas have twenty to a hundred cloud-free observations (Elvidge, et al., 2009). More precisely, the average number of observations is 39.2 with a standard deviation of 22 (Henderson, et al., 2012).

Table 2.1 shows the list of available composites per satellite-year. Note that when two satellites were orbiting at the same time, two different composites were produced. This creates a redundancy that can be used to intercalibrate the images, as we will see later in section 4.4. At the moment of writing there are 31 composites over a span of 19 years. It is not yet clear whether the database is going to be continued in this form or if a new ad-hoc mission will instead be started to get higher-resolution images.

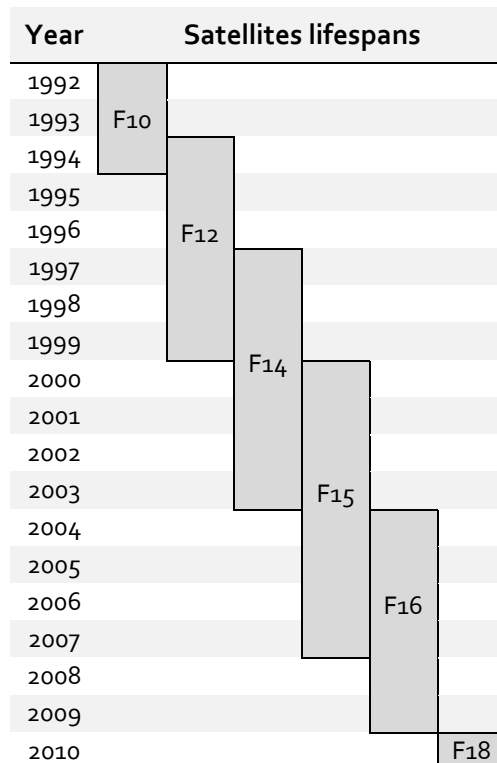


Table 2.1 - Visualization of available composites.
For most of the time, 2 satellites were orbiting on
the same time.

Every composite covers an area between 180 and -180 degrees longitude and -65 to 75 degrees latitude, i.e. some parts of Greenland, Alaska, Canada, Scandinavia and Antarctica are missing. However, it has been estimated that only about 10'000 people, or 0.0002% of the world population lives there (Henderson, et al., 2012).

The resolution is of 30 arc-seconds, which means that every pixel represents an area of about 0.86 square kilometers at the equator. The result are huge TIF images with an extension of 43'201 x 16'801 pixels, i.e. more than 725 megapixels. This is more than 100 times the amount of pixels needed for a good quality classical photo print of 11x14 cm.

Out of these composites, the following different products are available at the moment:

2.3.1 Cloud cover

As already described, the main purpose of the DMSP mission was to detect the cloud cover worldwide. The presence of clouds can be detected with the thermal sensor described above. These maps show how many observations were cloud-free for each pixel of the satellite-year composite, and can therefore be used to infer data quality.

2.3.2 Average lights x percentage

These products show the average Digital Number (DN) of nighttime lights, multiplied by the percent frequency of light detection. The original DN is assigned according to the cloud-free observations and it is quantified with 6-bit, i.e. the values range from 0 to 63. For unknown reasons, after the normalization with the percentage of detection, the pixel values were stored in float precision (32 bit), so that every composite weighs about 3 Gigabytes.

According to the NGDC, this product still contains a lot of background noise and ephemeral events like forest fires, so that it is not suited for the analysis of cities.

2.3.3 Stable lights

The main product of this database tries to measures the lights that are 'stable', i.e. areas that were lit most of the time. Considerable effort was devoted to reduce background noise and to remove transient events with median-like filters. Although most of the post-processing was done with algorithms, some parts of the noise reduction were done manually with the help of visual detection for areas that should be unlit, which most probably introduced some small artifacts in the images (see section 2.3.5). For a comprehensive description of the used methods see (Baugh, et al., 2010).

The quantization here is again 6-bits and the values are integers ranging from 0 to 63, this time stored as 8-bit Integers, for a total of about 700 Megabytes per image.

These products were improved over time and released in different versions. This is why I think it is important to mention which release was used for the analysis, which unfortunately isn't always the case in the literature (see Table 3.1 at page 20).

For example, in the CIESIN Thematic Guide to Night-time Lights (Doll, 2008), the stable lights product version 2 was described as 'frequency detection product', having a range from 0 to 100 (%).

2.3.4 Radiance calibrated data

The Digital Numbers (DN) does not correspond exactly to the physical amount of radiance received by the satellite for several reasons. The most relevant of them is the considerable amount of pixel saturation (DN=63) over very bright areas, such as big cities. An attempt (Elvidge, et al., 1999) to solve this shortcoming was made by changing the sensor gain of the satellite (sometimes even by a factor of 100), which was possible only for a limited amount of time. More images with different gain ranges were combined to obtain a better quantization (pixel values range from 0 to 6'030).

This product is better suited for quantitative analysis of the effective amount of radiation, and the following formula holds for the calculation of the actual Radiance:

$$\text{Radiance} = (\text{DN})^{3/2} [\text{Watts}/\text{cm}^2/\text{sr}]$$

This formula is based on a logarithmic scaling made by Elvidge in order to accomodate the range of the different radiances detected. No further details on this procedure or on the exponent are given.

Unfortunately, this product is currently only available for 2006 (apparently it was also available for 1996-1997 in the past, with a pixel value range of 0-255, (Doll, 2008)), so it is not suited for longer term time series analysis.

2.3.5 First comparison of the currently available products

To get an idea of the difference between the light maps, I compared the histograms of the three composite versions for the year 2006 (the only year available for the radiance calibrated product). The results are visualized as scatterplot in a log-log chart because otherwise, the shape of the distributions would not be visible.

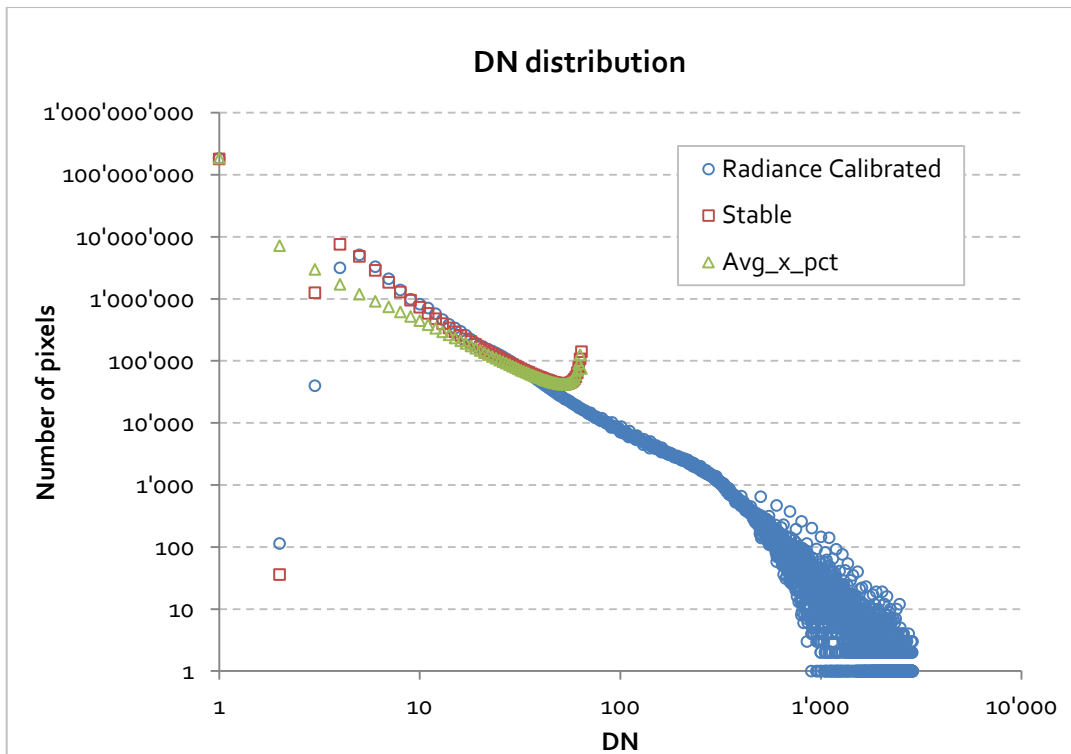


Figure 2.3 – Log-log plot of the DN intensity distribution of the three products for 2006, satellite F15

The first observation is that indeed, the radiance calibrated composite has a DN range which is two orders of magnitude larger than the other two. Another remarkable point is that the shape of all three distributions looks similar and it's almost a straight line with a negative slope. For the radiance calibrated and the stable lights product the slope is about -2, whereas for the Avg_x_pct product it is about -1.5 (these are just rough estimates based on least squares; in order to fit power laws, maximum likelihood methods should instead be used).

Another interesting fact is the upward shape of the tail for both the Stable lights version and the Average_x_percentage. This is most probably due to the saturation effect discussed before: pixels with high DN (>60) are way too frequent, especially if compared with the radiance calibrated version.

A strange artifact is visible in the initial part of the distribution for the stable lights and radiance calibrated products: the amount of dim lit pixels is unreasonably low. As already noted by other researches (e.g. (Henderson, et al., 2012)), this is probably due to the empirical operation of noise removal. A direct comparison between the stable lights and the average products, proposed in figure 2.4, shows however how the artifact is not limited to the first DNs but rather disseminated over the whole first half of the spectrum.

While it seems reasonable that during the removal of noise, a lot of dim pixels were lost, it remains unclear why there are no pixels with DN=1 and why the amount of pixels with DN between 4 and 30 is significantly higher than in the raw data of the avg_x_pct product.

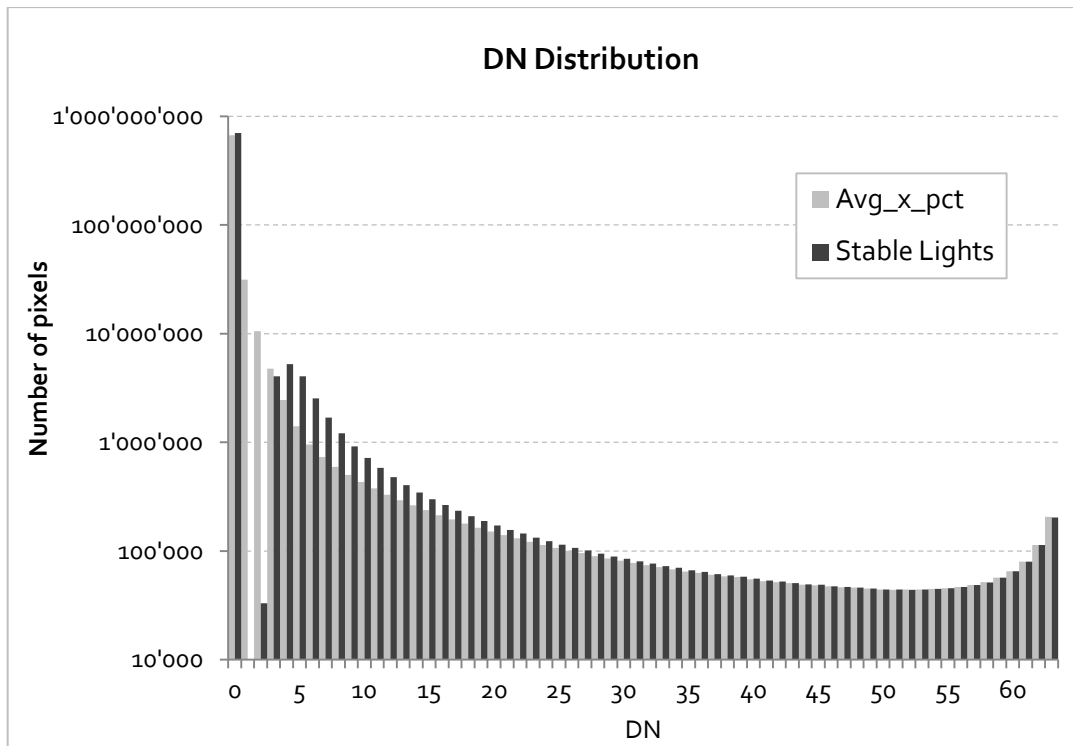


Figure 2.4 – log-lin histogram plot of the DN distribution in avg_x_pct and stable lights for the year 2000, satellite F14. Note the artifacts in the first half of the spectrum.

3 Past research

An important part of this research was devoted to the past literature on nighttime lights in order to get an idea of which applications of this dataset have already been studied. To the surprise of the writer and the supervisors, we stumbled upon a large research field with some hundred publications on a very broad variety of topics. The applications range from the estimation of economic indicators to the assessment of energy consumption, and from environmental issues to social ones. I'll try in the next pages to summarize the actual landscape of research based on this dataset.

3.1 Economic activity

One of the most popular applications is to use light as a proxy for the economic activity. Just by looking at the pictures it seems quite intuitive that there must be some kind of positive relationship between emitted light and level of economic development. Light comes mainly from nocturnal illumination of streets, buildings and industry areas, and since the resolution of the pictures is about 1 square kilometer, the light sources have to be very dense and constant to produce a bright pixel. Thus brighter pixels must indicate the presence of dense urbanized areas with potentially high population density (although the opposite is not always the case, as we will see).

Many studies try to estimate the total income, or Gross Domestic Product (GDP) of countries at different scales, in particular at a state and regional level. This is a very appealing application since official statistics are very hard to be collected with this granularity, especially for developing countries in Africa and Asia. One of the first attempts (Doll, et al., 2005) was made using the radiation calibrated product of 1996 and compared regional GDP data with the radiance detected at different scales of regional aggregation (For Europe, NUTS¹-levels 1 to 3) finding a very high positive correlation ($R^2=0.979$). The tests were made only in 11 European countries (GDP data from Eurostat) and in the U.S. (US Bureau of Economic Analysis).

Another attempt was made with the stable lights product of 2000 for the US, India, China and Turkey (Sutton, et al., 2007), also with the combination of population density measures, but the used method didn't seem to be significantly superior of official GDP statistics. Still, a significant log-linear relationship between light night energy and GDP was found ($R^2=0.74$). For the same countries and with similar methods, but starting from different products, other more sophisticated studies (Ghosh, et al., 2010) were made to obtain a better map of the regional economic activity. Other similar but country-specific studies were also conducted for China (Zhao, et al., 2010), India (Bhandari &

¹ Nomenclature of Territorial Units for Statistics, a geocode standard for referencing the subdivisions of countries for statistical purposes.

Roychowdhury, 2011) and Mexico (Ghosh, et al., 2009), always as a one-year snapshot and never using the time series.

More recent papers tried to consider the whole time span (Chen & Nordhaus, 2011) and (Kulkarni, et al., 2011) and conclude that light can be used as a proxy for economic activity but only for countries with the poorest statistical systems (or with very limited added value for countries with high-quality statistics).

Besides GDP, another important measure of economic statistics is the economic growth, usually intended as GDP growth. This is the subject of a more recent paper (Henderson, et al., 2012) which justifies the choice of this indicator with the fact that it is welfare-independent and much more convenient to compare across countries than nominal GDP. The authors try to estimate the growth of real GDP with a combination of light per area and national account statistics at national and sub-national level. As for the estimate of GDP, this approximation contains little added value for countries with high-quality income data, but for countries with low-quality income information, the optimal estimate puts roughly equal weight on lights growth and official statistics. For these countries, the growth estimates obtained differ substantially from the official ones. For example, in the last years Myanmar has an average annual growth rate of 10.02% according to the World Development Indicator of the World Bank (WDI), whereas the new combined indicator estimates only 3.26%. For Burundi, the WDI predict a GDP decline of -0.27%, whereas satellite data imply a growth of 2.89%.

To summarize, nighttime lights are a very appealing instrument to measure economic activity and economic growth. However, the relationship between the two indicators is highly complex, so that is difficult to get reliable estimations. Nevertheless, especially for countries with poor data quality, lights can *add* significant value to the existing statistics.

3.2 Population estimation

Another widely diffused application of nighttime lights is the estimation of population or population density at a high resolution. As already specified earlier, persistent light is an unequivocal indicator of the presence of human settlements, and where more light is produced, there should also be more people. One of the first attempts to model population density with nighttime lights (Sutton, 1997) used data from the 1990 U.S. census and a binary DMSP image showing only the saturated pixels. The model found however accounted only for 25% of the variation in the population density of the urban areas in the continental U.S.A.

A later study from the same author tried to estimate the global human population at country level, coming to a 1997 world estimate of 6.3 billion against the general accepted approximation of 5.9 billion (Sutton, et al., 2001)

Also here, specific studies were conducted at national level, e.g. for China (Lo, 2001) , (Zhuo, et al., 2009) and Brazil (Amaral, et al., 2006).

In conclusion, light alone may not be a perfect proxy to measure population, but combined with other sources it can substantially add value. It is worth noting that the Gridded Population of the World (GPW), one of the most widespread databases of the global population density, uses nighttime lights as one of the many inputs data.

3.3 Power consumption and distribution

Human-produced light, which is almost always the case for stable lighting², needs electrical energy or some sort of power source. Thus the Nighttime Lights database should provide a good approximation of where energy is available. The opposite statement is of course less reliable, i.e. we cannot really say that where there is no light, no electricity is available, mainly because of the relative coarse resolution of the images that cannot capture single and sparse light sources, but also because light may not be the primary or only one use of electricity. However, it was estimated that about 20% of the total world energy consumption is due to illumination (Efficient Lighting for Developing and Emerging Countries, 2012).

A first study showed very strong log-log correlation ($R^2=0.96$) between lit area and energy consumption at a country level (Elvidge, et al., 1997). Further similar studies were conducted at national level for India (Kiran Chand, et al., 2009), Brazil (Amaral, et al., 2005) and Japan (Letu, et al., 2010).

Another very interesting study explored the politics of electricity distribution in regions of India, where power as public good is a very scarce resource (Min, 2009). Although there is a relatively reliable network infrastructure, the actual power supply is by far not sufficient to satisfy the demand. The decisional power of giving energy to a certain municipality, district or county is quite centralized and involves political control. However, only a weak correlation could be found between availability of energy in the municipalities (lit pixels) and political party that won the elections.

Light is thus a quite good proxy for estimating *where* electricity is available, whereas it is a bit more delicate to infer the *amount* of energy consumed (mainly because of the saturation issue and different uses of energy). In order to analyze the temporal impact of politics and elections in developing countries, the time resolution of one year may be too coarse to detect changes: the process used to generate the year-composites may "average out" most of the relevant information needed.

3.4 Poverty and development index

Combining measures of economic activity and population, one can quickly come to other interesting measures like GDP per person or poverty ratio. A study in this direction (Elvidge, et al., 2009) was made by dividing the population count from Landsat by the average lights DN, which gives an idea of where people are living without (from the satellite detectable) light. The obtained Poverty Index (PI) was then calibrated by regressing it with the official statistics about the percentage of the population living with less than \$2 a day, aggregated at a country level. The obtained estimate of the number of people living in poverty was 2.2 billion, which is somewhat consistent with the 2.6 billion estimated by the World Bank.

² For a counterexample, see section 3.7 about gas flares



Figure 3.1 – Map of world poverty based on nighttime light. Brighter pixels indicate populated areas with proportionally few nighttime lights. Source (Elvidge, et al., 2009)

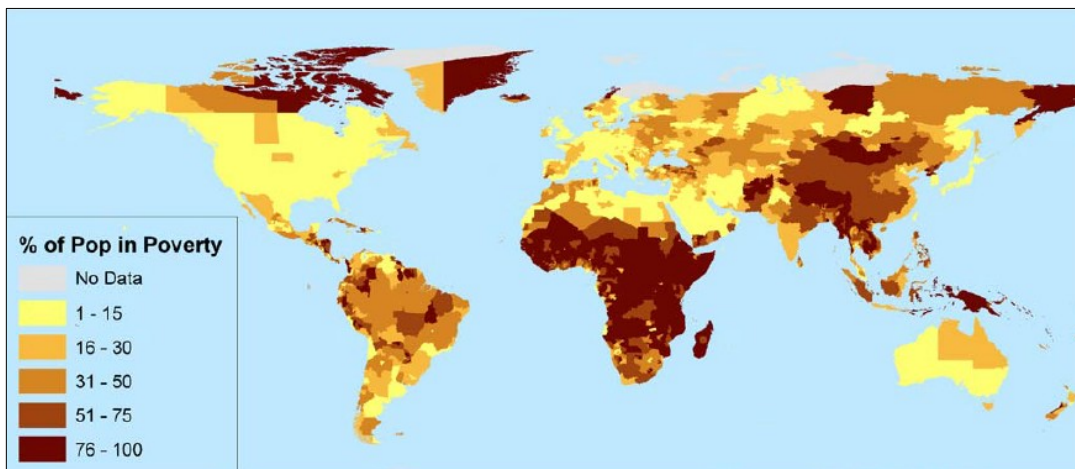


Figure 3.2 – Map of percent poverty levels for 2543 sub-national administrative units. The estimate is based on the satellite data-derived poverty index. Source (Elvidge, et al., 2009)

A later, more sophisticated attempt from the same authors to build a development index based on nighttime lights (Elvidge, et al., 2012) was made by building a spatial Gini-coefficient, which will be explained later in section 6.5.

This seems to be a very promising way to use the database, and the coincidence with other measures supports this feeling. We can indeed say that nighttime illumination is a major indicator of wealth and development.

3.5 Effects of wars

Some studies also tried to assess the effects of wars by means of the nighttime luminosity. Conflict-related events such as large fires that burn for weeks, large refugee movements but also destructive actions that cause power outages, and the subsequent reconstruction of the electricity distribution infrastructure, are detectable in the light maps.

One study evaluates the US military ‘surge’ in Iraq in 2007 (Agnew, et al., 2008), which was aimed to stabilize and rebuild the city after the war. The authors expected an increase in luminosity over time, thanks to the restoration of electrical infrastructure. However, no observable effect was found.

Another, more complete study looked for effects of the wars in Caucasus regions of Russia and Georgia (Witmer & Loughlin, 2011). The authors claim to be able to detect oil fires and large refugee outflows, as well as settlements (re)construction.

Again, as for the power consumption application, the time resolution of one-year may be in general too coarse to detect the actual impact of wars, but for large conflicts with a longer duration, light can be used to study damages and reconstruction dynamics.

3.6 Urban extent

Another widespread research topic is the validation of urban boundaries. Currently already more than half of the world population lives in cities (McKinsey Global Institute, 2012), and the percentage is growing. This faces policy makers to big challenges in the field of land use, the distribution of public goods and transportation infrastructures. Therefore an understanding of how cities spatially grow and evolve is needed.

One of the first attempts to map urban or densely populated land areas in the U.S. with the nighttime lights was made by just thresholding the DMSP/OLS images and comparing them with the official statistics (Imhoff, et al., 1997). A more sophisticated analysis, using also the radiance-calibrated version of the database, was made for three cities with different degrees of urbanization and development: Lhasa, San Francisco and Beijing. (Henderson, et al., 2003).

The spatial size-frequency distribution of settlements was also analyzed using different thresholds, with the interesting finding that conurbations larger than 80km diameter account for less than 1% of all settlements but for about half the total lighted area worldwide (Small, et al., 2005).

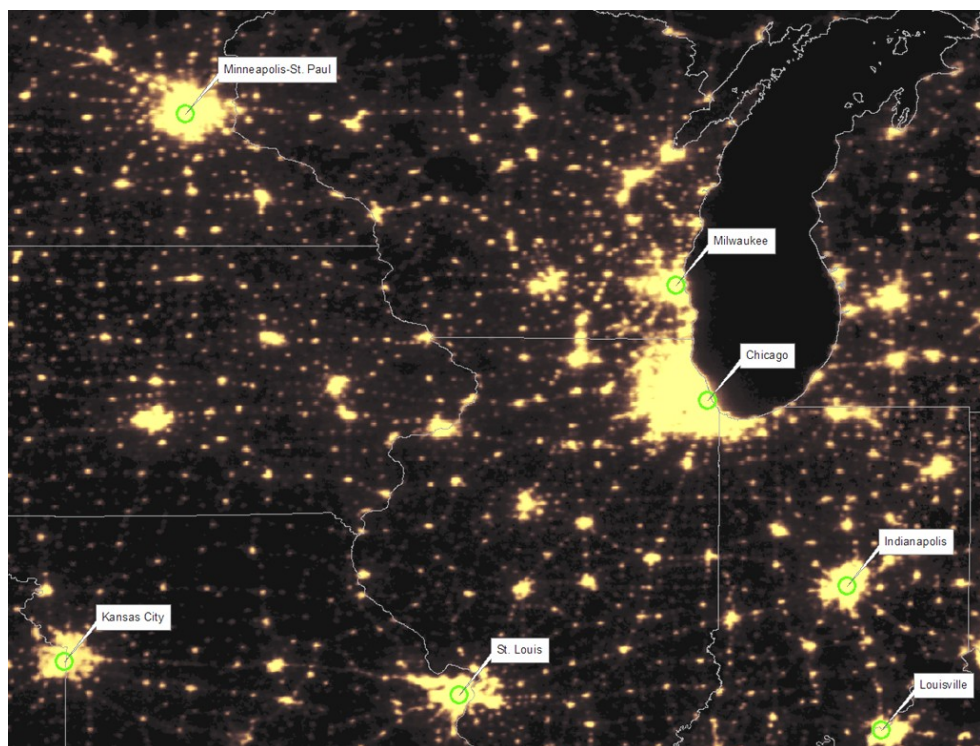


Figure 3.3 – City lights in the US (2009). The biggest cities are labeled.

Another specific paper studied the density of constructed impervious surfaces area (ISA) on earth (Elvidge, et al., 2007), finding that China has more ISA than any other country ($87'182 \text{ km}^2$, i.e. more than twice the total area of Switzerland). This motivates other studies on the land cover and the level of urbanization in that particular country (Lo, 2002), (Ma, et al., 2012).

Although lights slightly overestimate the urban extent because of blooming (over-spilling of luminosity around big cities and reflection near water bodies), the use of thresholds mitigates this drawback and makes this application a very promising research field.

3.7 Environmental issues

Until now we have looked mainly at social- and economically-related applications of this dataset, but other interesting facts about nature events and the human footprint on the planet are also recorded in nighttime lights.

3.7.1 Forest fires

As already mentioned, large forest fires (natural and human made) are also visible from the satellites, before the median filter is applied to remove temporary effects and obtain the stable lights map. Studies were made to monitor the surface of forest affected by fires in India (Kiran Chand, et al., 2007), Indonesia (Fuller & Fulk, 2010) and Brazil (Elvidge, et al., 2010).



Figure 3.4 – Forest fires in central Africa in 1992. No stable human settlement is present here. The product used is avg_x_pct, whereas the pixel intensity has been strongly enhanced to become visible.

3.7.2 Gas flares

Another less known, but very important aspect recorded in the light maps are the so called gas flares. Gas flares are combustion devices used mainly in oil wells and big offshore platforms to burn flammable gas (mostly methane) released during the operations of oil extraction. The gas is burned only for convenience, or for lack of infrastructure, so that the whole energy is wasted and huge amounts of CO₂ are released in the atmosphere. The monitoring of this harmful and quite uncontrolled activity is thus motivated by environmental and health concerns, besides energy efficiency reasons.



Most gas flares burn nonstop, hence this phenomenon is observable also in the stable lights version of the database. The main research in this topic uses nighttime lights to estimate the total volume of gas burned in gas flares.

The conclusion was that only in 2008, approximated 139 billion cubic meters gas were wasted, equivalent to 21% of the natural gas consumption of the U.S., with a potential retail market value of \$68 billion and an impact on the atmosphere of 278 million metric tons of CO₂ equivalent (Elvidge, et al., 2009).

Figure 3.5 – Flaring gases from an oil platform in the North Sea.
Source: Varodrig, Wikimedia Commons

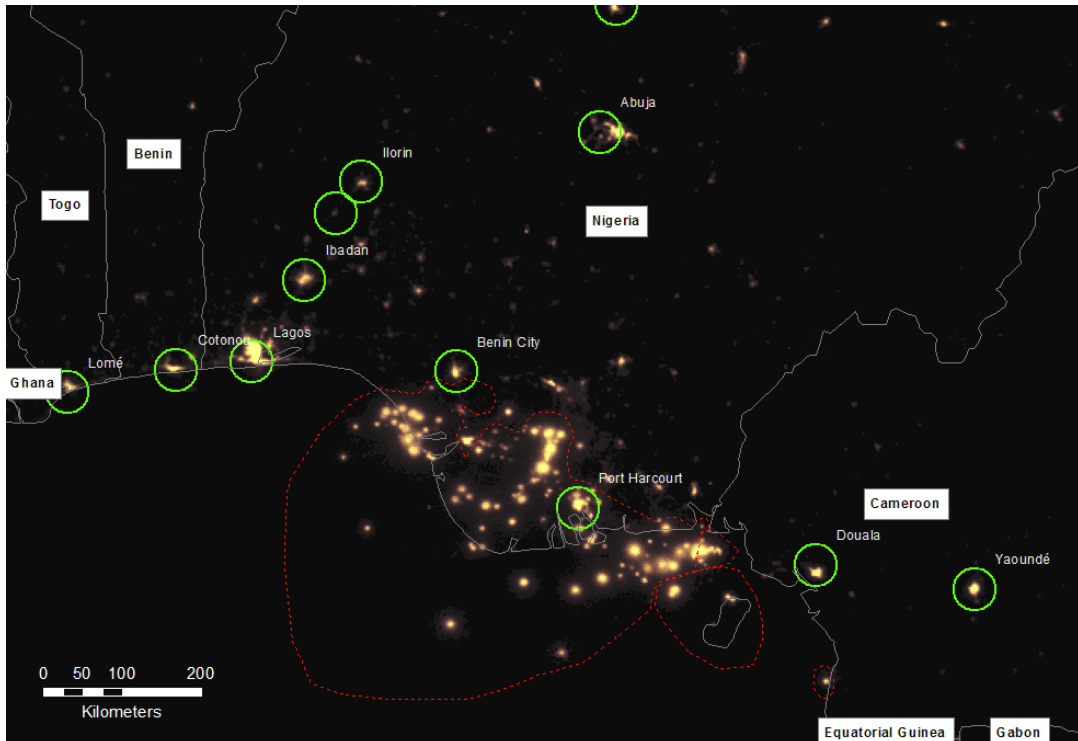


Figure 3.6 – Onshore and offshore gas flares in Nigeria in 2009 (red zone). Note the characteristic circular shape, and the remarkable size of the light footprint compared to the surrounding cities (encircled in green).

3.7.3 Fishing activity

It sounds incredible, but fishing boats can be seen from outer space. The main reason is that for some kind of fish, notably squid, fishing is done by night, and bright lights are mounted on the fish boats to attract more animals. This illumination is so intense³ and persistent that can be observed even in the stable lights version of the database.

Particular studies on this subject were made for Japan (Kiyofuji & Saitoh, 2004), where the spatial and temporal variability of nighttime fishing are analyzed to infer the migration and ecology of the squid, and for coral reefs worldwide (Aubrecht, et al., 2008), where nighttime illumination is seen as a stressor and a threat to the coral reefs ecosystems.



Figure 3.7 – Fishing boats in the sea between Japan and South Korea, in 1992

³ Also, water reflects and diffracts much of the light, which intensifies the amount captured by the satellites. Some kinds of lights are even mounted directly dozen meters under the water and point toward the surface.

3.7.4 Light Pollution

Light pollution is bad for at least three reasons: first, astronomical light pollution reduces the number of visible stars and disturbs the scientific observation of the sky. Second, the ecological light pollution represents a threat to entire ecosystems, substantially altering the behavioral patterns of the animal population (orientation, foraging, reproduction, migration, communication etc.). Third, wasted light means also wasted energy.

Some human health disorders were also found to be correlated with prolonged exposure to light during night, mainly because of alterations to the circadian rhythm.

The nighttime lights dataset show where the nighttime illumination is particularly strong, allowing to model the diffusion of light in the surrounding areas. Studies on this subject have been done for Europe (Cinzano, et al., 2000), (Cinzano & Elvidge, 2004) and Iran (Tavoosi, et al., 2009).

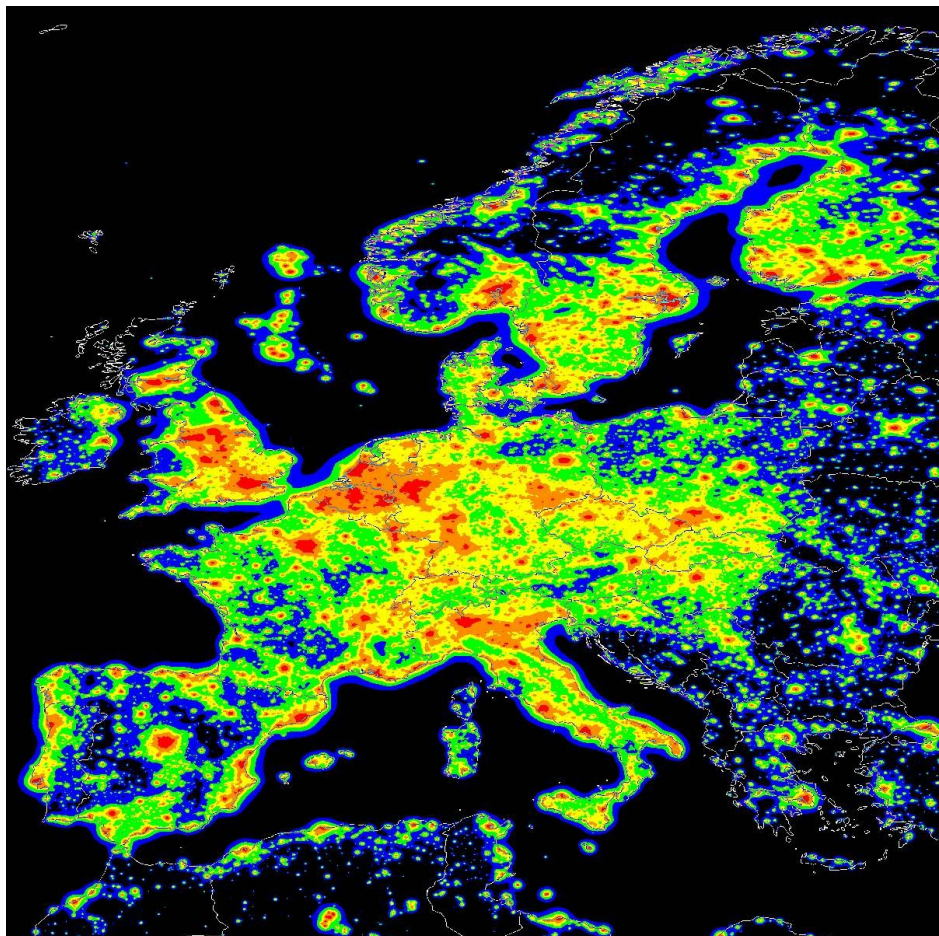


Figure 3.8 – Artificial sky brightness at sea level in Europe. In central Europe is almost impossible to find a spot with complete darkness. Source (Cinzano, et al., 2000).

In conclusion, nighttime lights can be very effectively used to assess the human footprint on the planet and the ecosystems. Among all the applications, light pollution is the most straight-forward and reliable one. The planning and the effectiveness of light-pollution abatement programs could be easily evaluated over the years with the help of this database.

3.8 Evaluation Table

In order to better understand the amount of preprocessing used in the literature, I prepared a table that shows which data and methods were used in the cited publications. The facts are inferred from the text of the research, i.e. if a procedure was not explicitly mentioned, it is assumed that it was not performed. Only the publications with a socio-economical motivation were considered in the table.

Application	Publication	Dataset version specified ⁴	Stable Lights	Radiance Calibrated	Avg x pct and variations ⁵	Single year	Multiple years	Intercalibration ⁶	Gas Flares Removed ⁷	Equal-area reprojection
Economic Activity	(Doll, et al., 2005)		x	x		x				x
	(Sutton, et al., 2007)		x			x				
	(Ghosh, et al., 2010)		x	x		x				
	(Zhao, et al., 2010)	2	x				x	x		x
	(Bhandari & Roychowdhury, 2011)		x			x		x	x	
	(Ghosh, et al., 2009),			x		x				x
	(Chen & Nordhaus, 2011)	4	x				x	x		
	(Kulkarni, et al., 2011)		x				x			
	(Henderson, et al., 2012)	4	x				x		x	
Population	(Sutton, 1997)		x			x				
	(Sutton, et al., 2001)				x	x				x
	(Lo, 2001)			x		x				x
	(Zhuo, et al., 2009)	2	x			x				x
	(Amaral, et al., 2006)		x				x			
Power Consumption	(Elvidge, et al., 1997)				x	x				x
	(Kiran Chand, et al., 2009)		x				x			
	(Amaral, et al., 2005)				x	x				
	(Letu, et al., 2010)		x			x				x
	(Min, 2009)		x				x			
Development Index	(Elvidge, et al., 2009)		x			x				
	(Elvidge, et al., 2012)			x		x			x	
Urban Extent	(Imhoff, et al., 1997)				x	x				x
	(Henderson, et al., 2003).		x	x		x				
	(Small, et al., 2005)				x		x			
	(Elvidge, et al., 2007)			x		x			x	x
	(Lo, 2002)			x		x				x
	(Ma, et al., 2012)	4	x				x	x		
TOTAL	27 publications	19%	63%	30%	18%	63%	37%	15%	15%	41%

Table 3.1 – Evaluation of data and methods used in the selected publications. Only a minority of the publications performed an accurate preprocessing of the database.

⁴ Left blank if not specified. The version refers normally to the algorithm used for detecting the stable lights

⁵ Apparently there were more different versions of the map using the frequency of detection as pixel value

⁶ For an explanation of the intercalibration between the satellite composite, see next section

⁷ Again, if the removal of gas flares was not explicitly mentioned, the cell is left blank

3.8.1 Discussion

As we can see from the table, the data sources used in the literature vary a lot. In the majority of studies the stable light version of the dataset was used, although unfortunately, most of the time no release version was specified. This makes a reproduction of the results often difficult, since only the most recent version is available for download. A smaller percentage used the radiance calibrated product (again, different versions were released as mentioned before), mainly with the motivation of quantitative measurements of the emitted energy and to avoid the saturation issues. Yet another portion of the studies used some version related to the frequency of detection. The tracking of the data sources was not easy at all because of the continuous improvements and releases of the database. Most products are not available anymore, making a comparison somewhat problematic.

An interesting point is that most of the studies considered just only one snapshot, although the images are available for many satellite-years. This is mostly motivated by the fact that the other datasets used to find the correlations are released less often.

Another quite surprising fact is that among all studies using more satellite-years, hence doing time series analysis or comparisons between different years, only very few (the most recent ones) performed some kind of cross-calibration of the images. It is known and documented (Elvidge, et al., 2009) that different satellites had different sensor settings (for example, F14 produced substantially dimmer images (Doll, 2008)), and even for the same satellite, in addition to the natural deterioration of the sensor over time, undocumented gain adjustments were made during the mission, so that the comparison between different image-years is really delicate. A quite new and widely accepted method for the intercalibration is presented in (Elvidge, et al., 2009) and will be explained in the next section.

Since for the applications mentioned in the table the gas flares are not relevant, they should be removed before performing any analysis. This operation was almost never done, or at least it was not mentioned explicitly in the publication. This phenomenon is present in at least 20 countries, notably Russia, Nigeria, Iran, Iraq and Algeria, and, especially for small countries (Qatar, Kuwait), it could lead to misinterpretation of the results, since gas flares can be easily confounded with small cities. It was calculated that in 2000, gas flares represented 3.2 percent of lights emanation worldwide, and in some regions as the sub-Saharan Africa (e.g. Nigeria) they accounted for even 30% of the total illumination (Henderson, et al., 2012).

The last preprocessing operation considered is the re-projection of the images with an equal-area method. This is always needed when analyzing spatial extent, because the pixels in the 30-arc second grid represent different land areas: for example, if one pixel at the equator represents 0.86 square kilometers, it denotes only 0.59 square kilometers it in London, at 51.5° Latitude.

Unfortunately, only in the minority of the publications satisfactory attention was given to these details. I tried to consider all of them during my research, as explained thoroughly in the next section.

4 Preprocessing

4.1 Software

Dealing with geographical images of up to 3 Gigabytes size is not trivial. Most commercial graphical editors have limitations in this sense and even the hardware architecture becomes a problem (in 32-bit operating systems, single processes can only use a maximum of 2 Gb of memory). Fortunately I could take advantage of the know-how of the research group of Prof. Heinimann and dive into the world of GIS.

GIS stands for Geographic Information System, and it is a quite broad concept. Usually it denotes an application system or a software package that can store, manipulate, analyze and display multiple geographical datasets like shapefiles (containing vector data as points, lines and polygons) and rasters (notably aerial photography or satellite imagery). These databases are mostly geo-referenced, i.e. they contain the geographical location of the represented information.

The software package used in the group is ArcGIS¹ from esri². ArcGIS is the world leading GIS software and it features a huge number of ready-to-use geoprocessing functions to process, edit and analyze different types of inputs.

One of the first functions which I could take advantage of was the implementation of the "pyramids": the bitmaps of the rasters are subsampled, smoothed and stored at many different resolutions, in order to save computational time later and allow real time editing with the graphical user interface. This facilitated a lot the first approach with the NGDC database.

For the automation of the many iterative processes, such as recurring calculations for every single raster, the integrated visual editor ModelBuilder was used. Most of the processing models created for the research are also reported as figures.

The analysis of the extracted data was performed mostly with MATLAB³ or Microsoft Excel.

¹ In my case, ArcGIS Desktop 10.0, Service Pack 5

² Environmental Systems Research Institute - <http://www.esri.com>

³ MATLAB 7.12.0

4.2 Product choice

After an attentive study of the literature and a consultation with the authors of the dataset, the best product type for a research about the spatial extension of cities seems, despite the small human-introduced artifacts described in section 2.3.5, the stable lights map. All the described methods and analysis from here onward refer therefore to the stable lights dataset, version 4 (NOAA National Geophysical Data Center, 2012). In total, 31 composites were downloaded, covering the years 1992 to 2010.

The country boundaries used in the whole research were downloaded as polygonal shapefile from CShapes (Weidmann, et al., 2010). This database includes also historical capitals and borders after the Second World War, but these data were excluded because out of the scope for this research. All countries that ceased to exist as geographical entities before 2008 (e.g. Yugoslavia, USSR) were removed from the shapefile, such that a total of 194 non-overlapping countries remained in the dataset.

Unfortunately, only during the final stage of my study, I discovered a few missing islands in this dataset, the largest ones being Puerto Rico ($9'104 \text{ km}^2$), Reunion ($2'512 \text{ km}^2$) and Guadeloupe ($1'626 \text{ km}^2$). The reason, according to the authors, is that they are not unambiguously identifiable as sovereign states. The results of both the global and the country-related analyses are nevertheless hardly affected by this issue.

For the geolocation of big cities, the point-based shapefile from (Nordpil, 2009) was used. It features the geolocated center of 589 cities with a population greater than 750'000 in 2010, plus the historical population count from 1950 until 2050 (projection) analyses.

4.3 Gas flares removal

As already explained, gas flares are a continuous phenomenon and thus their presence is recorded also in the stable lights. Since we want to study human settlements, they should be removed in order to avoid their misinterpretation as small cities or impervious constructed land. Gas flares are usually very bright and present a characteristic circular shape of saturated pixels, surrounded by a sort of glowing.

The most extensive study on gas flares (Elvidge, et al., 2009) lead to the estimation of their total volume and evolution, but also to a map featuring their location and extension. The group of shapefiles, one per country, was downloaded from the NGDC⁴ and then merged within ArcGIS. The obtained mask was then converted in a binary raster so that the gas flares locations had value zero whereas all others pixels had value one. Every stable light composite was then multiplied with this raster to obtain images free of gas flares.

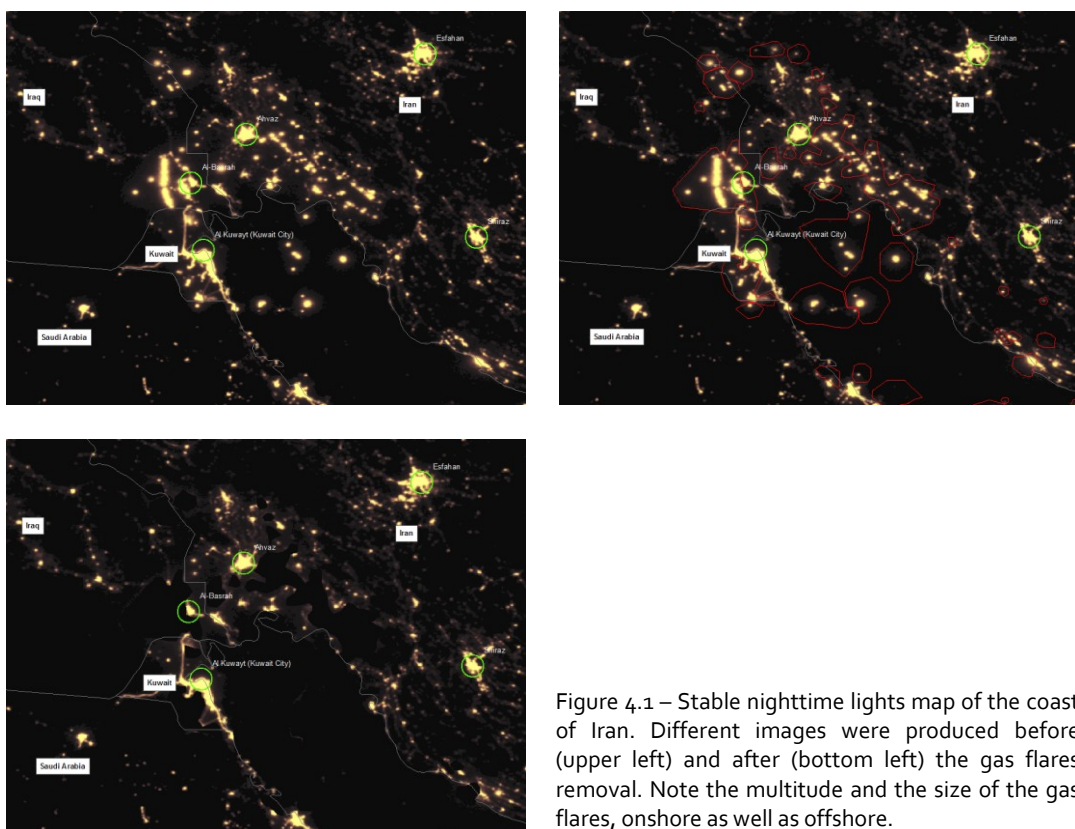


Figure 4.1 – Stable nighttime lights map of the coast of Iran. Different images were produced before (upper left) and after (bottom left) the gas flares removal. Note the multitude and the size of the gas flares, onshore as well as offshore.

Unfortunately, the polygons that encircle the gas flares are quite large. Thus it is unavoidable that certain areas of human-made lighting are canceled out, in particular if dim lit and when in proximity of gas flares. This drawback is however less incident on the amount of city lights than having the whole set of gas flares in the composites (see section 3.8.1).

⁴ http://www.ngdc.noaa.gov/dmsp/interest/gas_flares_countries_shapefiles.html

4.4 Intercalibration

As mentioned in the previous section, the satellite composite images are not cross-calibrated. Different satellites had different sensor settings, and even for the same satellite, in addition to the natural deterioration of the sensor over time, undocumented gain adjustments were made during the mission (most probably to enhance the detection of clouds, as this was the primary goal of the DMSP) so that the comparison between different image-years requires some caution.

An extensive study on that subject (Elvidge, et al., 2009) proposes an intercalibration based on an empirical process. It is a regression based technique, relying on the assumption that the illumination in a reference area has changed little over time. First, F121999 was chosen as base composite, because it presented the highest digital values in general. Then, a reference area was chosen as follows: all the pixels values of the region were plotted in a scattergram against the same pixels for F121999. Every outlier from the diagonal indicates a change in lighting, so the goal was to find an area with a cluster of points evenly stretched along the diagonal and with as few outliers as possible. Of all examined regions, Sicily was found to have the most favorable characteristics.

I did a small research about Sicily finding out that the population grew only of about 0.17% from 2001-2010 (Eurostat, 2012). The assumption that the illumination changed little over time there seems therefore to be somewhat justified. The selection of a reference sample is a major obstacle for the intercalibration process; a very recent research (Li, et al., 2012) proposed an automatic intercalibration algorithm which iteratively looks for outliers in the scattergrams and eliminates them from the sample group for the regression. The method seems to perform quite well, but it was developed only for the region of Beijing.

Therefore I decided to use the method of Elvidge, because it is full documented, complete and already cited in other studies. He developed a second order regression for each satellite year, based on the scattergrams of Sicily mentioned before, leading to the three calibrating parameters per image C_0 , C_1 , and C_2 that have to be applied as follows:

$$DN_{new} = C_0 + C_1 * DN_{old} + C_2 * DN_{old}^2$$

The intercalibration coefficients presented in the mentioned publication include only the years 1994-2008, but another, not yet published, paper from the same authors was found (Elvidge, et al., 2011), which provides coefficients from 1992 to 2009. So, only F182010 was discarded for the analysis.

Since the regression actually performs a histogram balancing (for the region of Sicily), it is not necessary to execute this costly computation on every pixel: each pixel with value DN_{old} will be transformed in pixel with value DN_{new} . To save computational time, I thus computed a lookup Table (LUT) of all DN for every composite, and then just applied the transformation to the images. Table 4.1 shows a colored visualization of the LUT.

F10	F10	F10	F12	F12	F12	F12	F12	F12	F14	F14	F14	F14	F14	F15	F15	F15	F15	F15	F16										
1992	1993	1994	1994	1995	1996	1997	1998	1999	1997	1998	1999	2000	2001	2002	2003	2000	2001	2002	2003	2004	2005	2006	2007	2004	2005	2006	2007	2008	2009
0	1	1	2	0	1	1	1	2	2	1	2	1	1	1	1	1	1	1	1	1	1	1	1	1	1	1	1		
1	2	3	2	3	3	2	2	3	3	3	3	2	3	2	3	2	3	2	3	3	2	3	2	2	2	2	3		
2	3	4	4	4	4	3	3	3	4	4	4	4	4	4	4	4	4	4	4	4	4	4	3	4	3	3	3		
3	4	5	5	5	5	4	4	4	6	6	6	6	6	5	5	5	4	4	4	6	5	5	5	4	5	4	5		
4	6	6	7	6	6	6	5	5	8	7	7	6	6	6	6	5	5	5	5	4	5	4	5	4	5	5	6		
5	7	7	8	8	7	6	6	10	9	9	8	8	8	7	7	6	6	9	8	7	7	8	7	6	6	7			
6	8	9	9	7	8	7	6	6	10	9	9	8	8	8	7	7	6	6	9	8	7	7	8	7	6	7			
7	10	10	8	9	8	7	7	11	11	10	9	9	8	8	8	7	7	10	9	9	9	8	8	7	7	8			
8	11	11	9	10	10	9	8	8	13	12	11	10	10	9	8	8	8	11	10	10	10	11	9	11	8	9			
9	12	13	13	14	14	14	14	14	14	13	12	11	11	11	11	11	11	11	11	11	11	11	11	11	11	11			
10	14	14	11	13	13	11	10	9	9	14	14	13	12	11	11	10	10	10	11	11	11	11	11	11	11	11			
11	15	15	12	13	14	13	12	11	17	15	15	14	13	13	12	11	11	16	14	14	14	15	12	11	11	12			
12	16	16	13	14	15	14	13	12	18	18	17	16	15	14	14	13	12	12	17	15	15	15	16	13	12	12	13		
13	17	18	18	14	16	16	15	14	20	19	18	17	16	15	16	14	13	18	17	16	16	16	17	15	13	14	15		
14	19	19	16	17	17	16	15	14	21	21	19	18	17	17	15	15	14	20	18	17	17	16	18	16	13	14	15		
15	20	21	17	18	18	17	16	15	23	22	21	20	19	18	16	16	15	21	19	19	19	19	20	17	14	15	16		
16	21	22	18	19	19	18	17	16	24	23	22	21	20	19	17	17	16	22	20	20	20	21	18	15	16	17	18		
17	22	23	19	20	21	19	18	17	25	25	24	23	22	21	20	19	18	23	22	22	22	22	22	22	22	22	23		
18	24	20	21	22	20	19	18	17	26	26	25	24	23	22	21	20	19	23	22	22	22	22	22	21	21	21	22		
19	25	25	21	22	23	24	23	22	21	30	30	29	28	27	26	26	25	28	27	27	27	27	27	27	27	27	28		
20	26	26	22	23	24	23	22	21	31	31	30	29	28	27	26	26	25	29	28	28	28	28	28	28	28	28	29		
21	27	27	23	24	25	23	22	21	30	30	29	28	27	26	26	25	25	29	28	28	28	28	28	28	28	28	29		
22	28	28	24	25	26	24	23	22	32	32	31	30	29	28	27	26	26	32	31	30	30	30	29	29	29	29	30		
23	29	29	25	26	27	25	24	23	34	34	33	32	31	30	29	28	27	32	31	30	30	30	29	29	29	29	30		
24	30	30	26	27	28	26	25	24	35	34	33	32	31	30	29	28	27	35	34	33	33	32	32	32	32	32	33		
25	31	31	27	28	29	27	26	25	36	35	34	33	32	31	30	29	28	35	34	33	33	32	32	32	32	32	33		
26	32	32	28	29	30	29	28	27	36	35	34	33	32	31	30	29	28	36	35	34	34	33	33	32	32	32	33		
27	33	33	29	30	31	29	28	27	37	36	35	34	33	32	31	30	29	37	36	35	35	34	34	33	33	32	33		
28	34	34	30	31	32	30	29	28	38	37	36	35	34	33	32	31	30	38	37	36	36	35	34	34	34	33	34		
29	35	35	31	32	33	31	30	29	38	37	36	35	34	33	32	31	30	39	38	37	37	36	35	35	34	34	35		
30	36	36	32	33	34	32	31	30	40	39	38	37	36	35	34	33	32	40	39	38	37	36	35	35	34	34	35		
31	37	37	33	34	35	33	32	31	40	39	38	37	36	35	34	33	32	40	39	38	37	36	35	35	34	34	35		
32	38	38	34	35	36	34	33	32	41	40	39	38	37	36	35	34	33	41	40	39	38	37	36	35	34	34	35		
33	39	38	34	35	36	34	33	32	41	40	39	38	37	36	35	34	33	42	41	40	40	40	41	37	33	34	36		
34	40	39	35	36	35	34	33	32	42	41	40	39	38	37	36	35	34	43	42	41	42	42	43	40	36	37	38		
35	41	40	36	37	38	36	35	34	43	42	41	40	39	38	37	36	35	44	43	42	43	42	43	40	36	37	38		
36	42	41	37	38	39	37	36	35	44	43	42	41	40	39	38	37	36	45	44	43	44	45	44	41	37	38	39		
37	43	42	38	39	40	38	37	36	45	44	43	42	41	40	39	38	37	46	45	44	45	46	45	42	38	39	40		
38	44	43	39	40	41	39	38	37	46	45	44	43	42	41	40	39	38	47	46	45	44	45	46	43	39	40	41		
39	45	44	40	41	42	40	39	38	47	46	45	44	43	42	41	40	39	48	47	46	45	46	47	44	40	41	42		
40	46	45	41	42	43	41	40	39	48	47	46	45	44	43	42	41	40	49	48	47	46	47	48	45	41	42	43		
41	47	46	42	43	44	42	41	40	49	48	47	46	45	44	43	42	41	49	48	47	46	47	48	45	42	43	44		
42	48	47	43	44	45	43	42	41	50	49	48	47	46	45	44	43	42	51	50	49	48	47	48	45	42	43	44		
43	49	48	44	45	46	44	43	42	51	50	49	48	47	46	45	44	43	52	51	50	49	48	49	46	43	44	45		
44	50	49	45	46	47	45	44	43	52	51	50	49	48	47	46	45	44	53	52	51	50	49	50	47	44	45	46		
45	51	50	46	47	48	46	45	44	53	52	51	50	49	48	47	46	45	54	53	52	51	50	49	47	44	45	46		
46	52	51	47	48	49	47	46	45	54	53	52	51	50	49	48	47	46	55	54	53	52	51	50	48	45	46	47		
47	53	52	48	49	50	48	47	46	55	54	53	52	51	50	49	48	47	56	55	54	53	52	51	50	47	48	49		
48	54	53	49	50	51	49	48	47	56	55	54	53	52	51	50	49	48	57	56	55	54	53	52	51	48	49	50		
49	55	54	50	51	52	50	49	48	57	56	55	54	53	52	51	50	49	58	57	56	55	54	53	52	50	49	51		
50	56	55	51	52	53	51	50	49	58	57	56	55	54	53	52	51	50	59	58	57	56	55	54	53	51	50	51		
51	57	56																											

It is important to mention that the calibration introduces substantial alterations in the histograms. Entire ‘columns’ are shifted from one DN to another, sometimes merging, so that the actual probability distribution is slightly transformed (Figure 4.3).

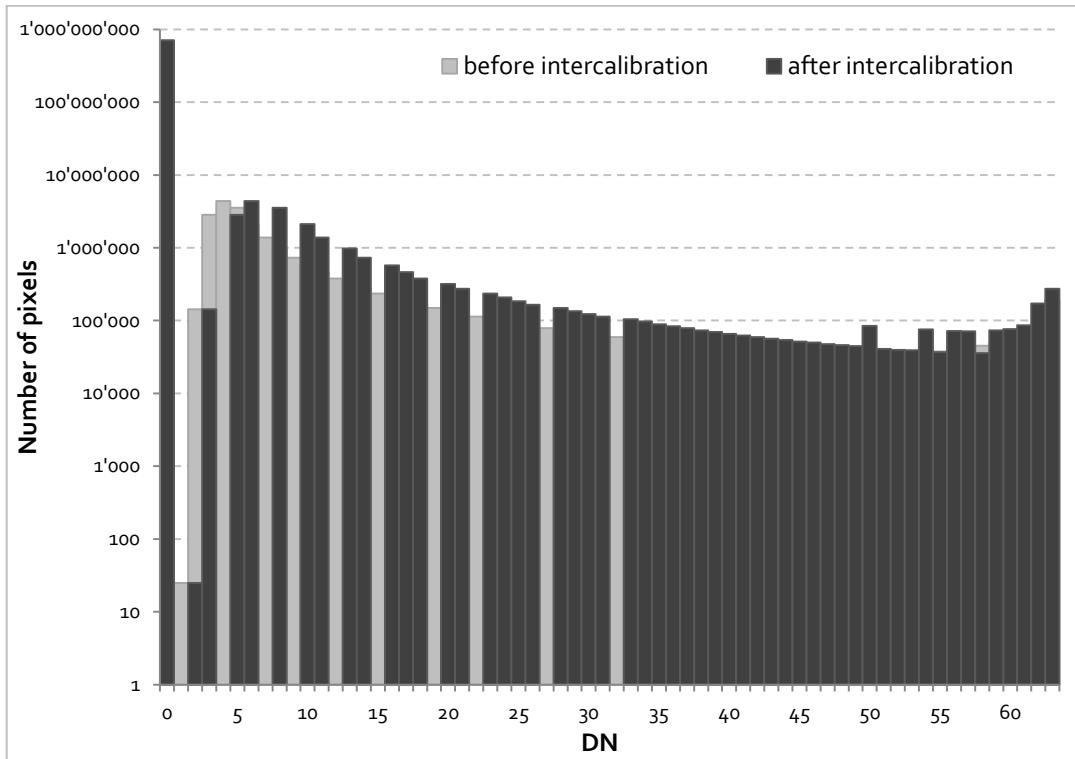


Figure 4.3 – Log-lin histogram plot of F141997, before and after the intercalibration. Note how entire columns of the histogram have been displaced (DN 1 to 2, 2 to 3 etc.), producing some ‘holes’.

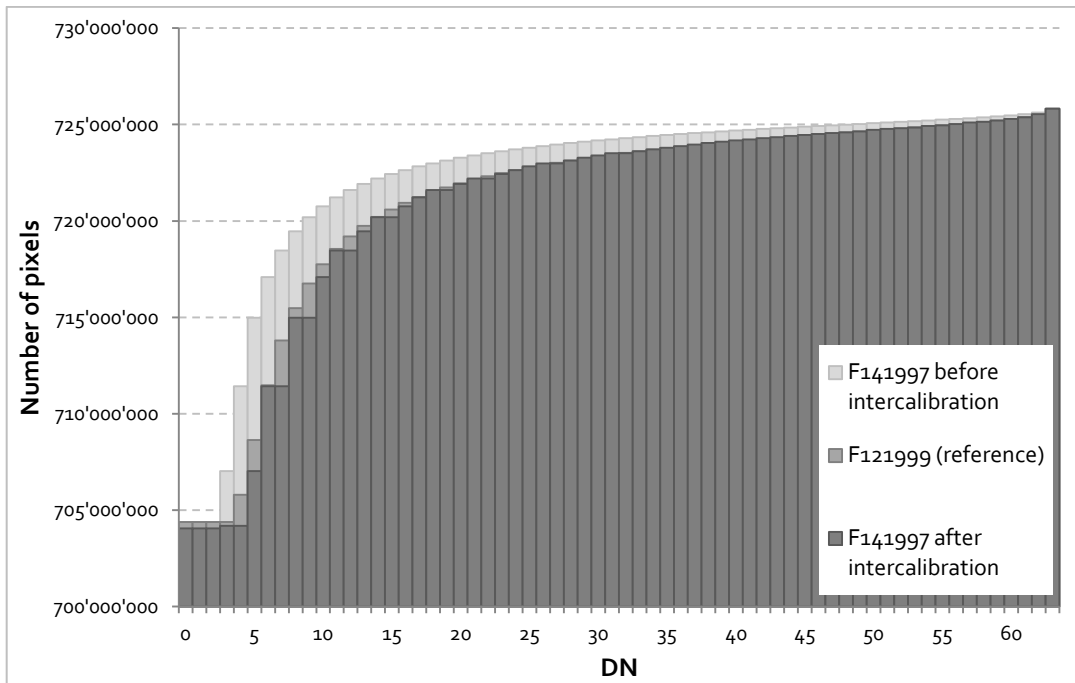


Figure 4.4 – Cumulative histogram of F141997, before and after the intercalibration. The last column is equally high reflecting that the total amount of pixels didn’t change. After the intercalibration, the cumulative histogram looks much more like the one of the reference composite F121999.

An indicator of the goodness of the calibration is that the Sum of Lights (SOL), i.e. the sum of all pixel values for a certain region, matches between two composites of the same year coming from different satellites. Figure 4.7 shows the example of China.

A perfect consistency is not obtained: the author of the calibration claims that this could be due to yet other differences in the sensor settings or also to slightly different times at which the pictures were taken from the satellites. Nevertheless, the result looks definitely better than without calibration.

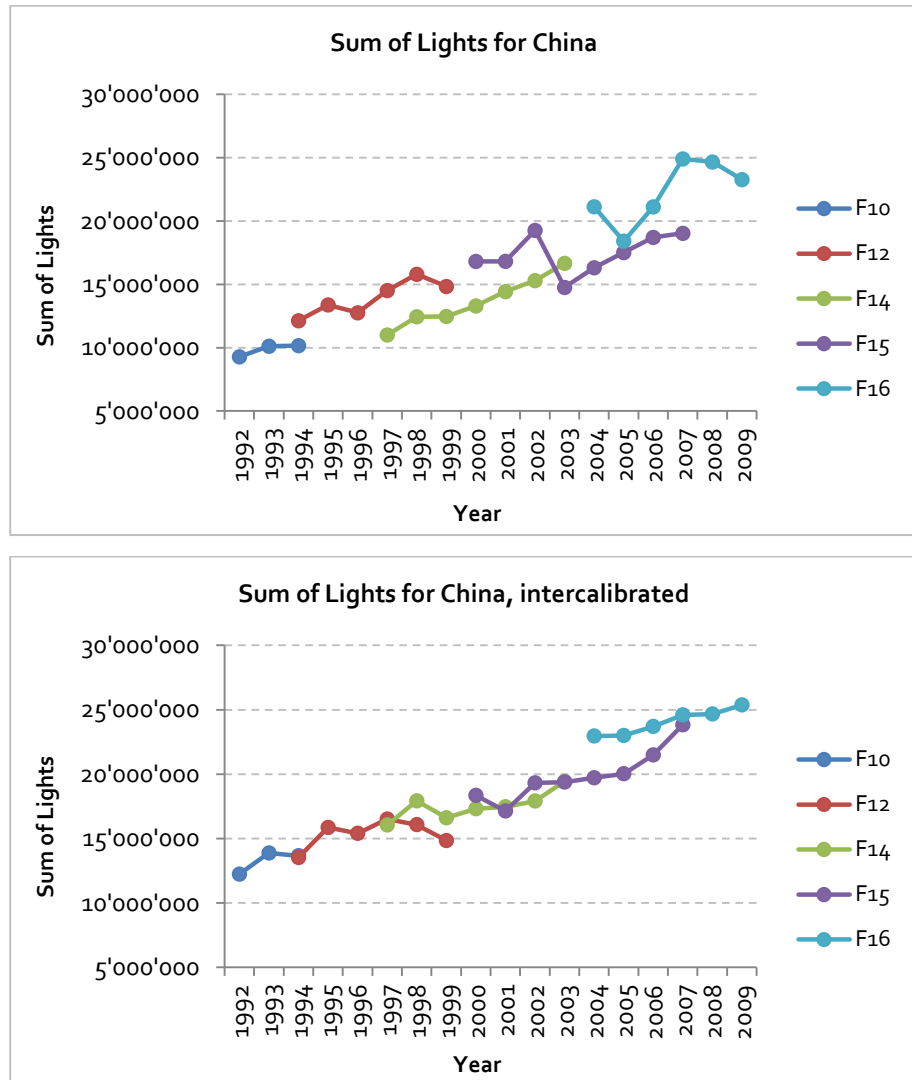


Figure 4.5 – Sum of lights for China. Note the difference between before (top) and after (bottom) the intercalibration

4.5 Reprojection

The 30 seconds arc grid used in the composite is not equal-area, i.e. one pixel doesn't always represent the same amount of land surface. In Quito (on the Equator), one pixel represents approximately a square with 952m per side, i.e. 0.86 square kilometers, whereas in Reykjavik (64°N latitude) it represents a rectangle about half so high, or a surface of 0.41 square kilometers. Since we want to analyze the spatial extent of cities, the equal-area property is needed.

For this purpose, the Mollweide⁵ projection was chosen. It is a pseudo cylindrical map projection where the accurate representation of areas takes precedence over the shape. The resulting images have a shape of an ellipse with the two extremes portion cut out. The resampling technique used was nearest neighbor, which is the best suited for integer inputs, and the chosen cell size was 1'000x1'000 m, i.e. one square kilometer per pixel.



Figure 4.6 – Mollweide projection of the stable lights from F101992

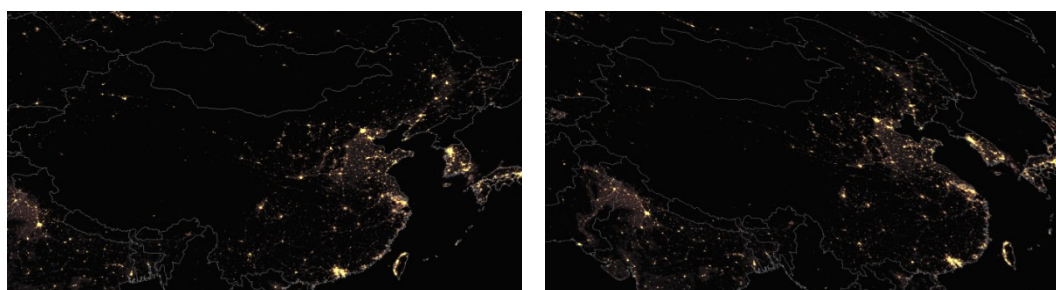


Figure 4.7 – China before and after the reprojection. Note how the country shape is distorted.

⁵ From Karl Mollweide (1774-1825), German mathematician and astronomer which, among other things, invented the homonymous map projection.

4.6 Average satellite/year

After intercalibration and reprojection, it is now meaningful to average composites of the same year made from different satellites. This way we obtain 18 composites, one for every year between 1992 and 2009.

For this purpose I just calculated every pixel as an arithmetic average between the two images with the Raster Calculator tool.

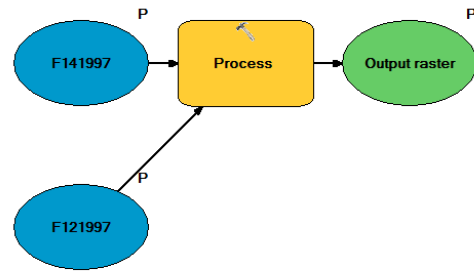


Figure 4.8 – Model for averaging two satellite images of the same year

Figure 4.7 shows again the example of China, after the reprojection and the averaging procedure. Note that the sum of Lights is substantially lower because the reprojection enlarged the cells from a variable area of 0.5-0.8 square kilometers to equal cells of one square kilometer.

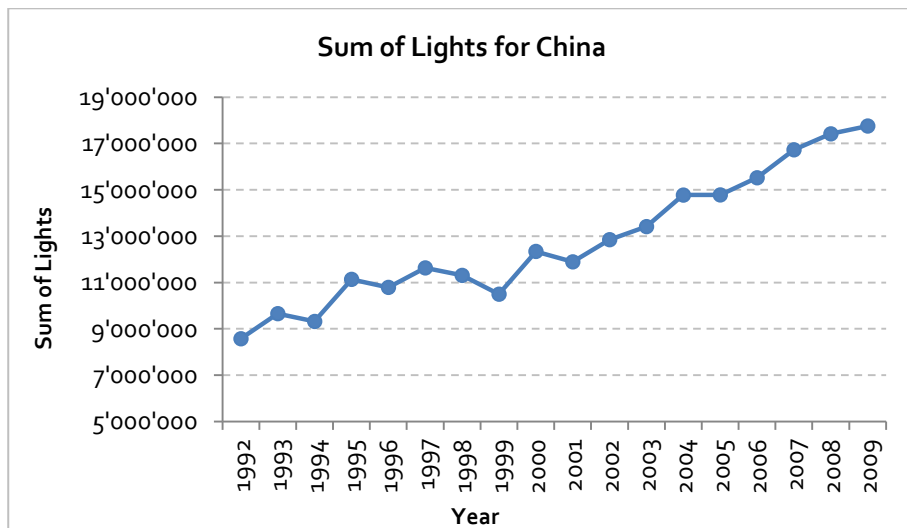


Figure 4.9 – Sum of lights for China after averaging. It has more than doubled in the last 18 years.

5 Mean center of lights

Where is the center of gravity of the light emissions worldwide? Is it moving, and if yes, in which direction and at which speed? This is one of the research questions that arose during the analysis of the nighttime lights dataset.

5.1 Motivation

The idea comes from a research of the McKinsey Global Institute called 'Urban World: Cities and the rise of the consuming class' (McKinsey Global Institute, 2012) . It presents a method to calculate the economic center of gravity of the world by weighting countries locations (center of landmass) by GDP and project the results on the earth's surface.

The research uses data and approximations from the year 1 until 2010 and makes a projection until 2026. It shows how the center of gravity (located near Kabul at year 1) shifted toward the north-west till about 1950 (Reykjavik), but is rapidly moving back to the east since the last 50 years, and with an incredible pace. In fact, they estimate that the shift occurred between 2000 and 2010 was the fastest ever since.

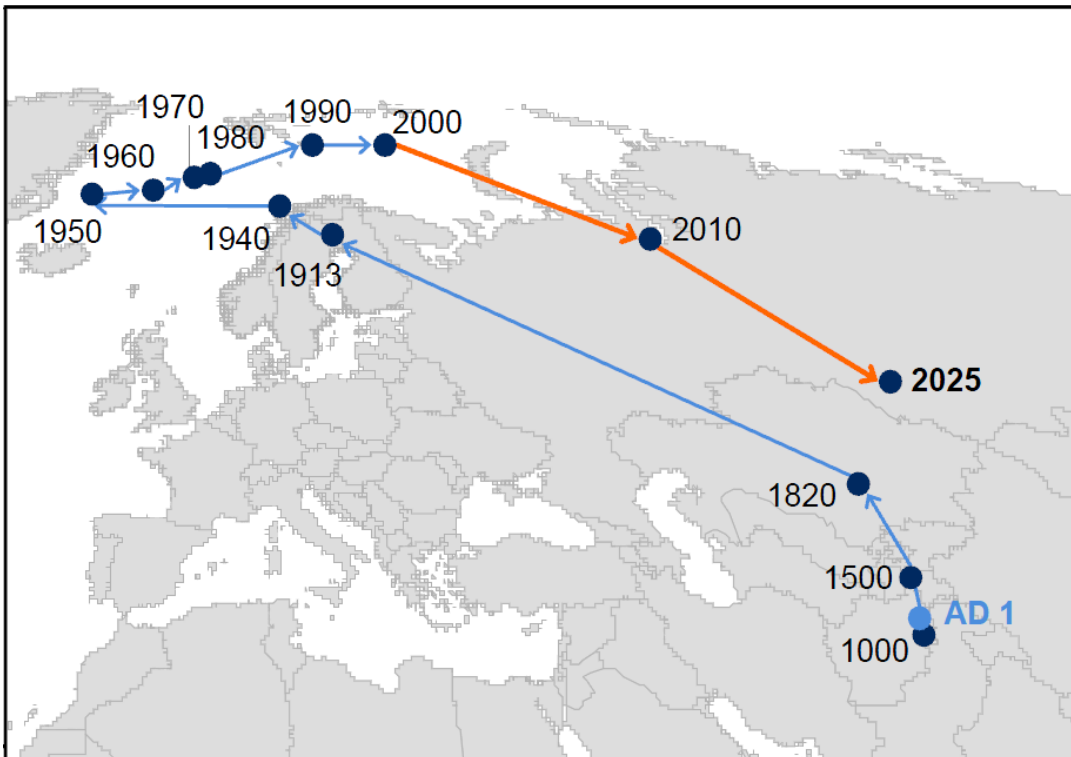


Figure 5.1 – Global center of gravity (GDP based) from year 1 to 2010, and projection for 2025. Source: (McKinsey Global Institute, 2012)

5.2 Method

In order to perform a similar test with the amount of nighttime lights, I used the function 'Mean Center' of ArcGIS. Since the function doesn't accept rasters as input but only feature classes with attributes as weights, I had to aggregate the amount of luminance at a country level. This was made by summing up all the pixel values within the country borders. The result was saved for every country and for every satellite-year in the countries shapefile. In order to produce more points and to get an impression of how well the intercalibration performed, the procedure was executed prior to averaging the images of the same years (see paragraph 4.6).

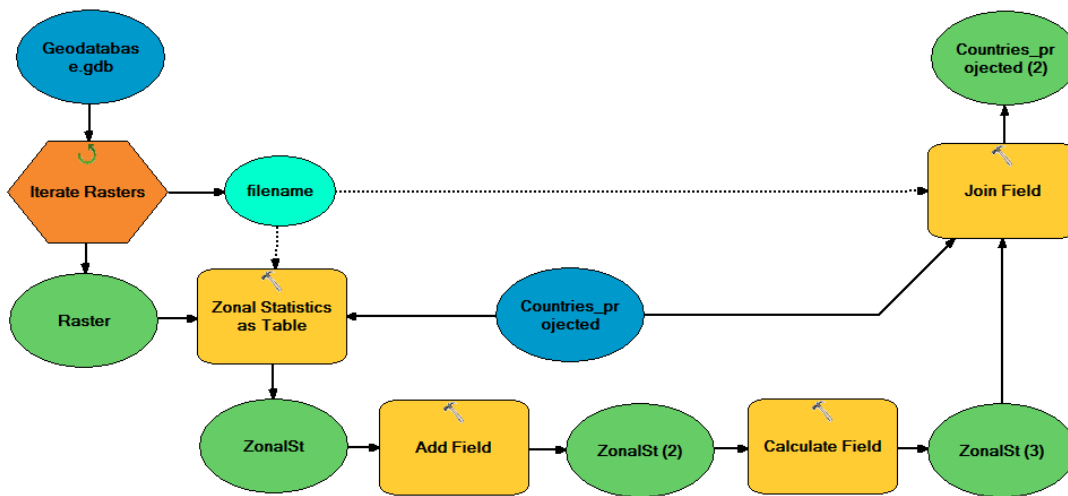


Figure 5.2 – Model for the computation of the sum of lights at a country level for every composite

After that, the mean center was calculated with the countries shapes as input and the sum of lights as weighting. Since it was problematic to iterate over different fields of the same table, a simple model was generated and then run multiple times with a batch.

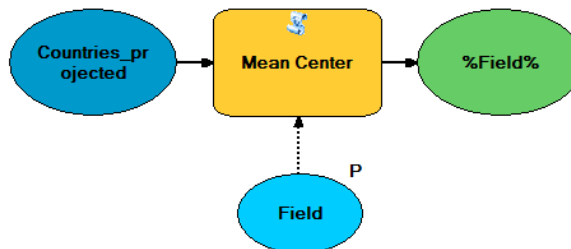


Figure 5.3 – Model for the computation of the Mean Center. The iteration was performed with a batch job.

All the centroids obtained were then merged into one single layer. The points were colored and labeled according to satellite, respective year.

5.3 Results

The overall location of the mean centers differs substantially from the results of McKinsey. I believe that this is mostly due to differences in the projection of the coordinates and the calculation of the center of landmass, but could also have other reasons inherent to the nature of nighttime lights in comparison to GDP.

The direction of the movement instead seems to be consistent with the map proposed by McKinsey: there is a clear shift toward south-east, although the amplitude of the movement appears a little smaller (~1'000 km). The speed of that shift is difficult to assess, however it looks like in the earlier 90' the movement was somehow quicker than after 2000, which would be inconsistent with the findings of McKinsey.

The reason for the shift moving also to the south and not only toward the east is probably that in the three dimensional space of the globe, the two driving powers China-India and USA don't only lie "next" to each other (longitudes) but also slightly "across" (latitudes).

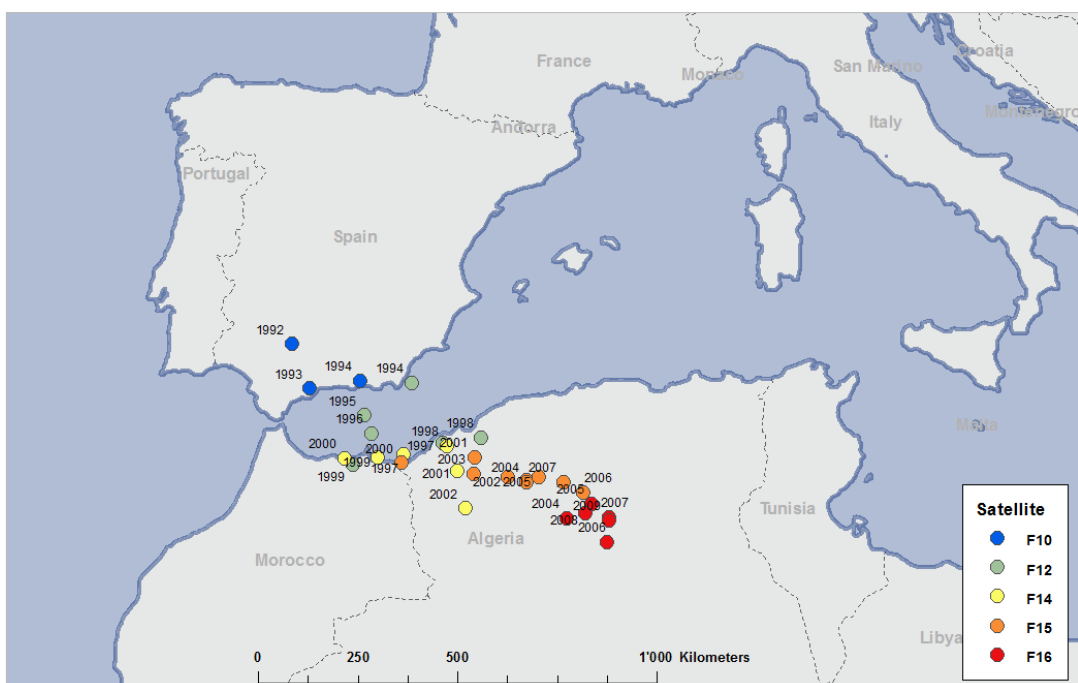


Figure 5.4 – Light mean centers per satellite/year. Note the strong shift toward East. The amplitude of the movement is of about 1'000 km, i.e. roughly half the estimate of McKinsey.

The intercalibration described in section 4.4 doesn't produce perfectly overlying centroids for the composites of the same year produced by different satellites. However, a comparison with a test performed prior to the cross-calibration shows that the dispersion of the points is significantly lower after this step.

Figure 5.5 shows the same map where the centroids are calculated on the average sum of lights per satellite, in order to emphasize the south-east direction of the shift. To avoid the expensive operation of generating new rasters, the average sum per country for every satellite was computed separately and the obtained table was then joined to the original shapefile of the countries. The same model as in figure 5.2 was then run again on these new attributes.

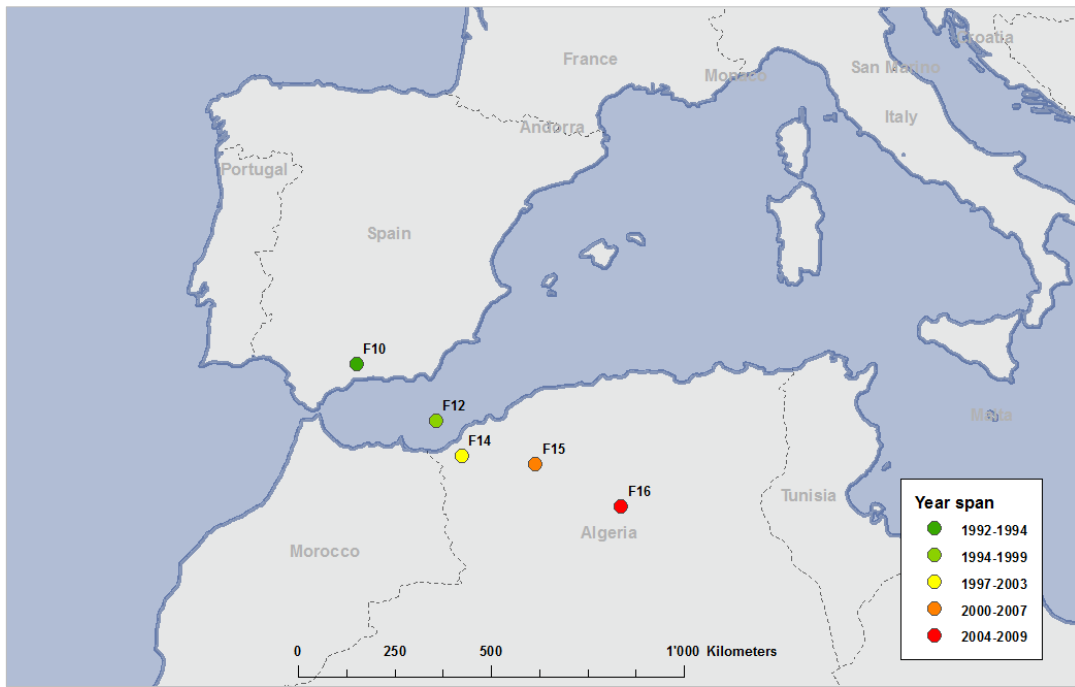


Figure 5.5 – Light mean centers per satellite. The centroids are here calculated on the average sum of lights per satellite (labeled), in order to emphasize the direction of the shift. Each satellite covers the year span indicated in the legend, as already described in the table 2.1.

6 Spatial light Gini

6.1 Motivation

Another method to study the distribution of lights is to look at their level of dispersion, or 'inequality'. The intuition is that some countries will show a stronger '*centralization*', i.e. a large amount of bright lit pixels and a small amount of dim lit ones, whereas other, more '*democratic*' countries, will present a more uniform distributed illumination with a lot of dim lit pixels over their territory.

Can we recognize this kind of configurations with the help of nighttime lights? Can we understand and categorize the organization dynamics of cities in different kinds of countries?

6.2 Methods

To evaluate the level of inequality I chose the Gini coefficient¹, which is a measure of statistical relative dispersion, initially developed to study the disparity in the distribution of income. The easiest way to understand the Gini coefficient is by means of the Lorenz Curve, which displays the cumulative distribution function of wealth (in the original version) versus the cumulative percentage of population, allowing statements like "the poorer x% of the population gets y% of the wealth". A Lorenz curve along the diagonal indicates therefore complete equality, i.e. everyone gets the same share of income².

The Gini coefficient is calculated as the ratio of the area that lies between the diagonal and the Lorenz curve over the total area under the diagonal (see Figure 6.1). A coefficient of zero indicates thus total equality, i.e. everyone gets the same amount of wealth, whereas a coefficient of 1 indicates total inequality, i.e. only one person gets all the income.

Since every measure is relative and expressed in percentage, the Gini coefficient is not only income-independent, allowing the comparison between countries with different levels of income, but also independent from the population size.

¹ From Corrado Gini (1884-1965), an italian statistician, demographer and sociologist who developed this indicator, later named after him.

² Note that the graphical representation can produce artifacts in this special case, depending on the chosen granularity. For example, if the graph is plotted only by steps of 10%, we can only state that 10% of the population gets 10% of the income. On the other way, if everyone gets indeed the same amount of income, the Lorenz curve will necessarily correspond to the line of equality.

In our case, the quantity observed is not wealth but light, and the population count is the amount of pixels, or square kilometer cells, i.e. the geographical dispersion. Our 'Spatial Light Gini' measures therefore how light is spatially distributed over the area of a country.

Again, because the measures are normalized, we can use our coefficient to compare countries with very different level of luminosity and very different areas.

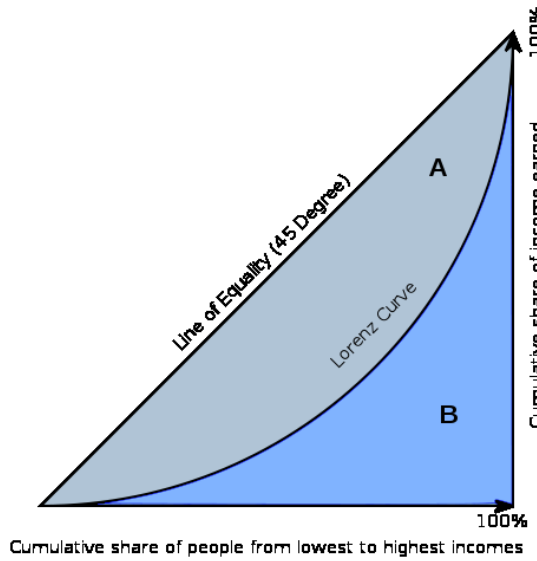


Figure 6.1 – An example of the classical Lorenz curve. The Gini coefficient is defined as $A/(A+B)$. Source: Wikipedia.

The computation of the Gini coefficient can be performed in many different ways. I chose a version which takes as input a discrete probability function, and not a list of samples, because handling every single pixel as an input would be computationally too expensive (recall that every image has 725 million pixels, see section 2.3). Also, ArcGIS provides geoprocessing functions to export directly the histograms.

Given a discrete probability function $f(y_i)$, where y_i are the points with nonzero probabilities, indexed in increasing order ($y_i < y_{i+1}$), we can compute the Gini coefficient G with the following formula:

$$G = 1 - \frac{\sum_{i=1}^n f(y_i)(S_{i-1} + S_i)}{S_n}$$

Where

$$S_i = \sum_{j=1}^i f(y_j) y_j \quad \text{and} \quad S_0 = 0$$

To extract the discrete probability function from the composite I created a model that computes the histogram of every country for every year. This is done with the help of the processing function 'Zonal Histogram' (Figure 6.2). The result is exported in a Database file (DBF) that can be read by Excel and MATLAB.

For the analysis, the histogram is then converted in a discrete probability function by simply normalizing the amounts to obtain frequencies that add to 1 (Figure 6.3).

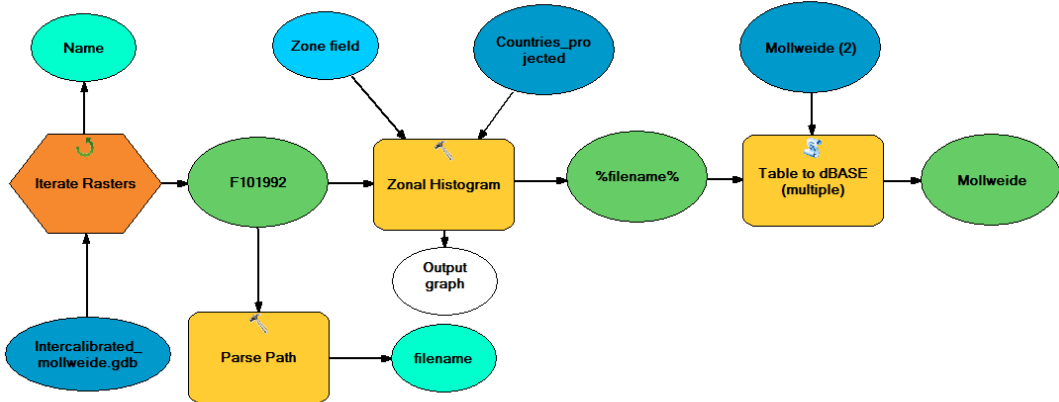


Figure 6.2 – Model for exporting the histograms to DBF. The operation is performed for every country (zonal histogram), and for every composite (iterator). The histograms are stored as tables with the following structure: the first column contains the histogram labels, i.e. the light values. The following columns, one per country, contain the amounts of pixels having the according value.

```

% Takes a matrix of histogram amounts and normalize them by dividing each
% column by the total of that column

function freq = to_frequency(input)

a = sum(input);
totals = repmat(a,size(input,1),1);
freq = input./totals;

```

Figure 6.3 – MATLAB function to compute the frequencies out of the histogram amounts.

```

% Function to calculate the Gini coefficient taking as input an histogram
% INPUTS  x_values : the labels of the histograms values (y)
%         hist      : the amount (count) for every value (f(y))
% OUTPUT   G        : the Gini coefficient

function G = light_gini(x_values,hist)

% converts the histogram counts in frequencies
list = to_frequency(hist);

% computes f(y)*y
s = list.*x_values;
% computes the cumulative summation
s = cumsum(s);

% workaround to get S0=0
s2 = [0; s];
s = [s; 0];
% get the second part of the numerator
s3 = s+s2;

list = [list; 0];

% compute the Gini coefficient
G = 1 - sum(list.*s3)/s2(end);

```

Figure 6.4 – MATLAB code to compute the Gini coefficient. The calculation follows the formula presented in the previous page, taking as input a histogram table.

6.3 Results

As figure 6.5 shows, the Gini coefficients differ substantially from one country to another. For example, the Netherlands have a very low Gini coefficient whereas Brazil shows almost complete inequality.

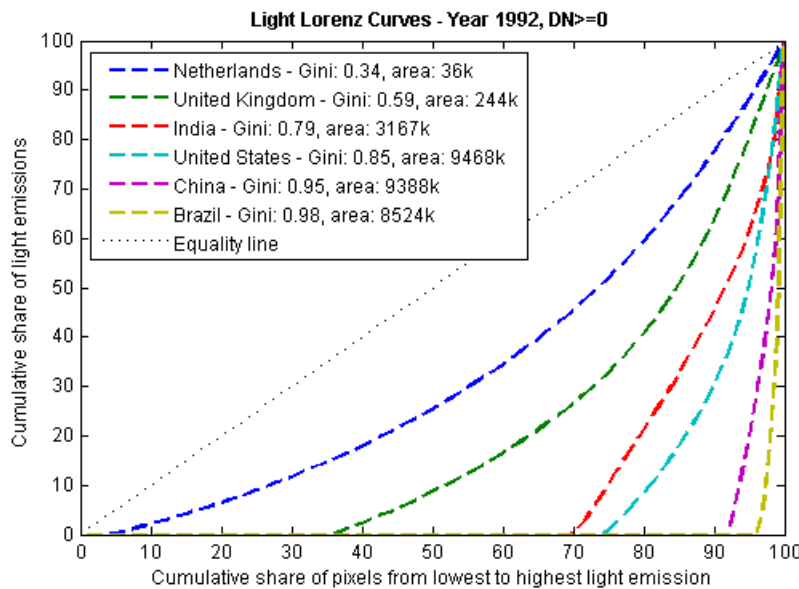


Figure 6.5 – Lorenz curves and relative Gini coefficients for selected countries in 1992. The variable ‘area’ indicates the amount of square kilometers (in thousands) considered, which in this case coincide with the land area; this measure differ slightly from the official numbers, most probably because of the level of precision of the borders shapefile used.

However, an important caveat hides behind this chart: although the Gini coefficient allows comparing countries with different land area, such a measure doesn’t account for the portion of land that *cannot* be inhabited/illuminated. For example, a huge portion of Brazil is covered by the Amazonian forest which of course is not urbanized, whereas the surface of the Netherlands is almost completely habitable.

To overcome this drawback, I eliminated from the evaluation all the cells that aren’t lit at all, i.e. with DN=0. This way we compare the distribution of light intensity only among cells that are lit, hence performing another sort of ‘normalization’. The curves look completely different now and the gap between countries has almost completely disappeared, as figure 6.6 shows. The range of the Gini coefficients goes now only from 0.32 to 0.41. This is quite astonishing, especially if we compare the considered area: the United States off America has a lit area which is more than 70 times the one of the Netherlands, but despite that, their Lorenz curves looks pretty similar and the Gini coefficients don’t differ much.

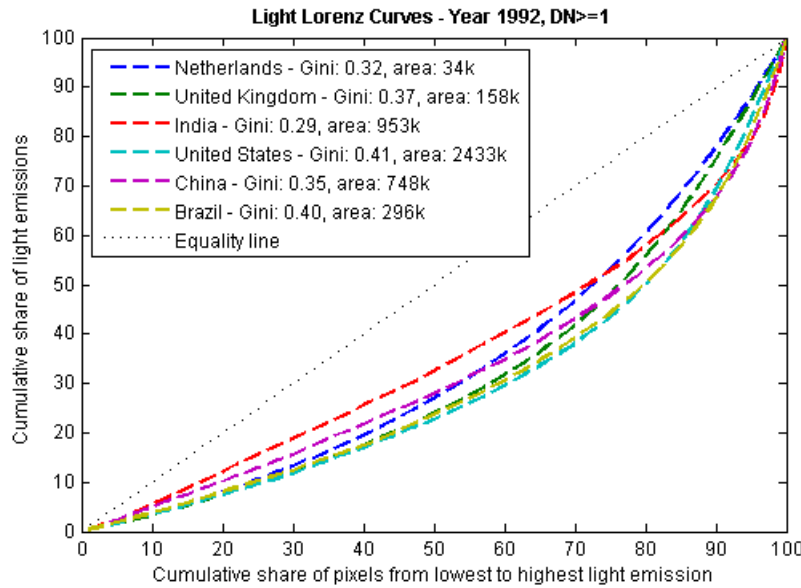


Figure 6.6 – Lorenz curves and relative Gini coefficients for selected countries in 1992, with threshold 1. This time, only lit pixels were considered: the variable 'area' indicates the amount of lit surface (in thousand square kilometers). Note how the curves are now very narrow and the Gini coefficients close to each other, around 0.35.

If we go even further, excluding the cells that are dimmer than a certain threshold, we consider only the more densely urbanized areas. Figure 6.7 show how quickly the Gini coefficient converges to the same value for every country.

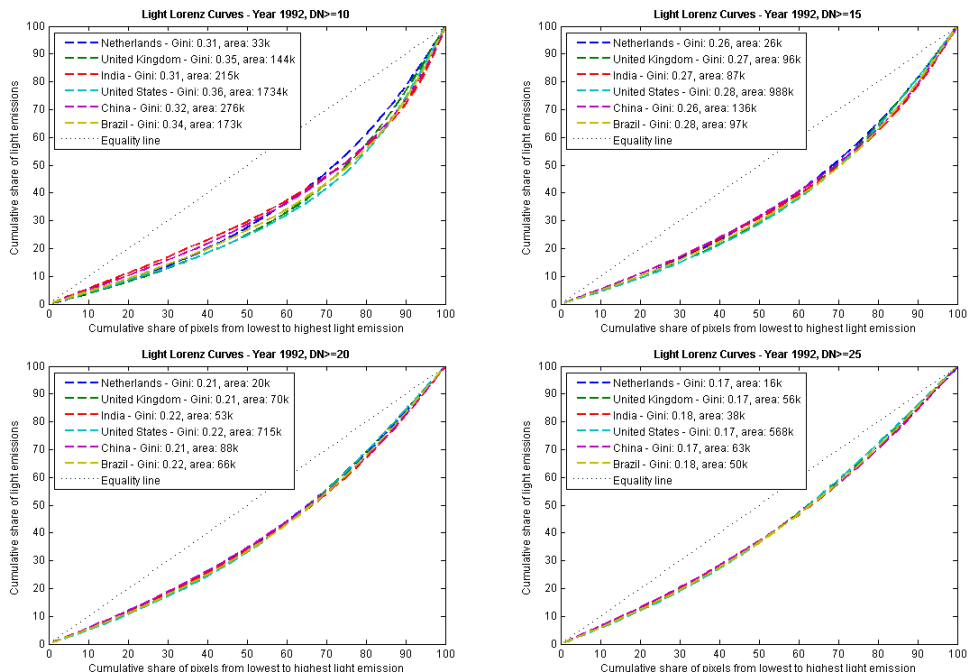


Figure 6.7 – Lorenz curves and relative Gini coefficients for selected countries in 1992, with increasing thresholds. Note how the curves become similar and the Gini coefficient converges to the same value. At the threshold of DN>=25, the Netherlands and United States have the same Gini coefficient, although the considered lit area still differs by a factor of 35.

This experiment indicates a sort of universal ratio between very bright cells and dimmer ones, or otherwise said, the spatial configuration of the settlements seems to follow a very similar pattern in every country. The hypothesis that more ‘democratic’ countries present a more equal distribution of light is rejected, and another observation arises instead: if we consider only the relatively dense urbanized areas, their spatial distribution is almost the same in every country, although the considered area can differ by up to two orders of magnitude.

Figure 6.8 shows how the Gini coefficients converge by increasing the threshold. Note that even the highest threshold tested, i.e. DN>25, is not even at the half of the spectrum of the light maps (0-63). Among the same selection of country, the mean and standard deviation of the Gini coefficients were calculated in function of the threshold used (Figure 6.9). Of particular interest there is the fall of standard deviation after the removal of the unlit pixels (DN>0).

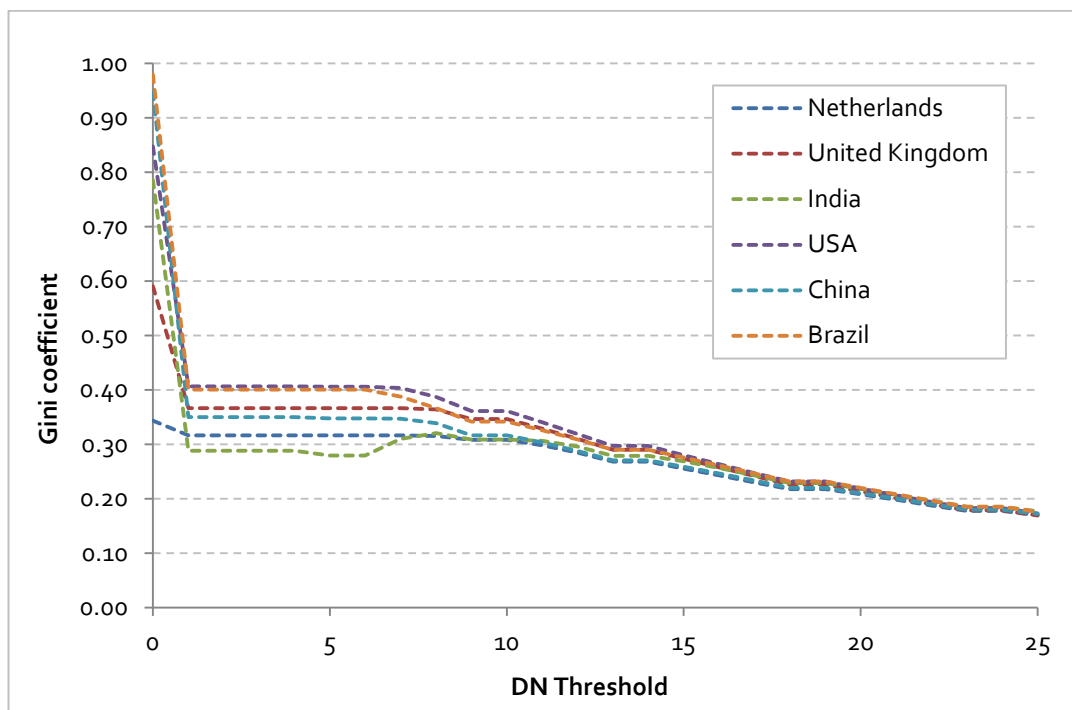


Figure 6.8 – The change in the Gini coefficient for selected countries in 1992 using increasing thresholds.

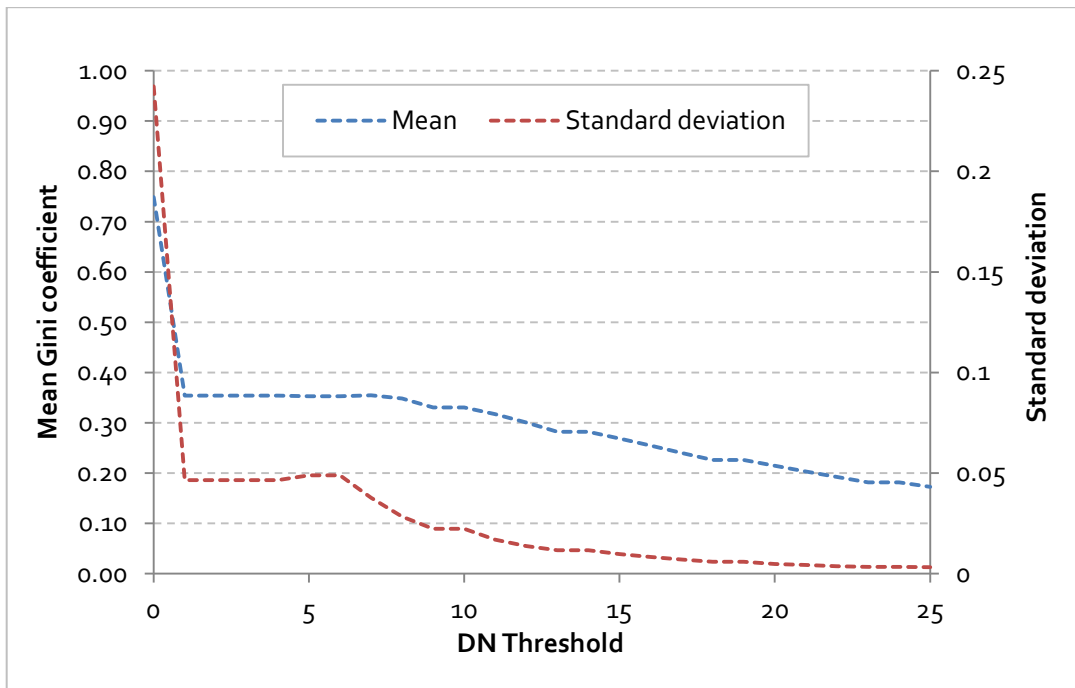


Figure 6.9 – Mean and standard deviation of the Gini coefficients as function of the threshold. The selection of countries is the same as in the Figure 6.8. Particularly interesting is the big jump on standard deviation from ~0.25 to only 0.05 by eliminating the cells with DN=0.

6.4 Evolution over time

Interesting is now to look at the evolution of the Gini coefficients over the years. The “naïve” version of the light Gini, i.e. without any thresholds, looks quite constant over time. This doesn’t surprise much, since especially for large countries, the result is always dominated by the vast amount of non-habitable land and thus unlit pixels, which drive the coefficients up.

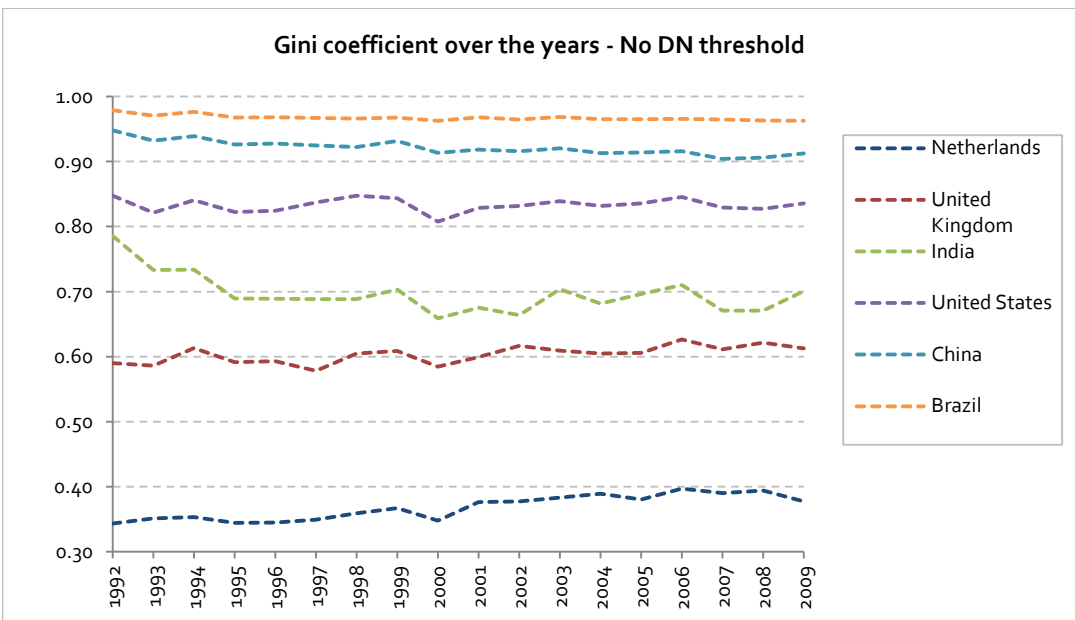


Figure 6.10 – Gini coefficients for selected countries over the years, without threshold

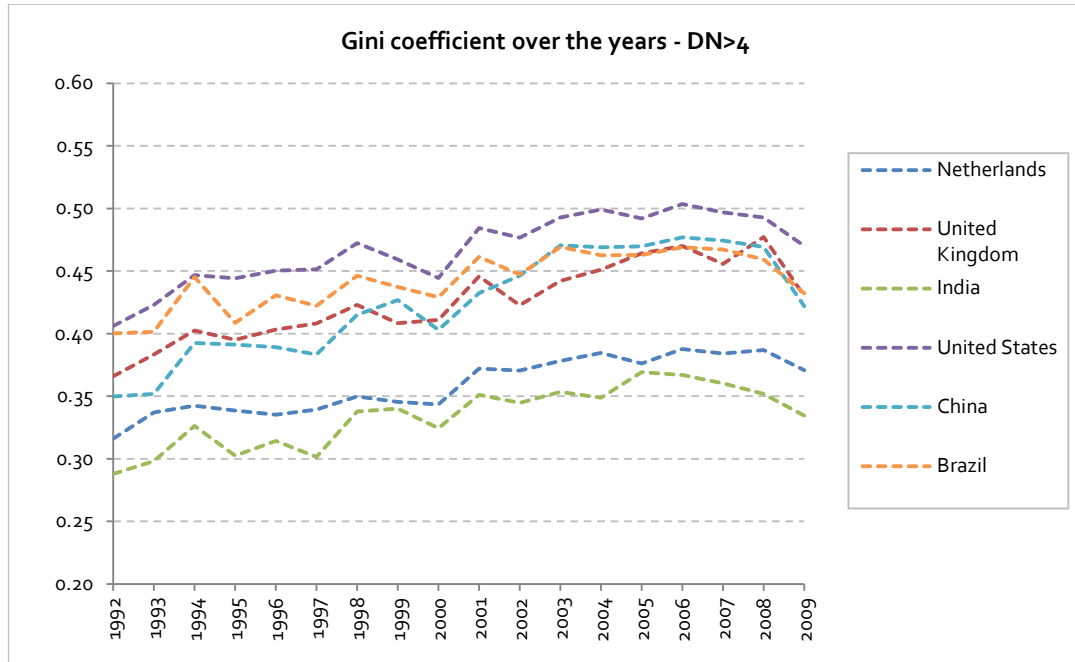


Figure 6.11 – Gini coefficients for selected countries with a threshold of $DN>4$. The threshold was chosen in order to keep as much information as possible, but to avoid at the same time the artifacts due to the intensity distribution in the lower DN (see section 2.3.5). Note the slightly upward trend.

The “normalized” version offers a different view: the Gini coefficients are very similar in every country and show a slightly increasing trend in the last 18 years. This suggests that the inequality in the spatial light distribution increased, or in other words, brighter pixels accounts for a relatively greater part of the luminosity. This can be explained by following scenarios:

- 1) The *area* that is dim illuminated increased proportionally more than the brighter one. The relative bigger quantity of dim lit pixels drives the Gini coefficient up, since the inequality is bigger. This would signify that villages and small settlements have been built (respectively electrified) over a surface greater than the one occupied by the city growth.
- 2) The *brightness* of the cities increased proportionally more than the brightness of small settlements. Assuming for example that the illuminated area didn't change, in order for the Gini coefficient to rise, the brighter pixels have to increase their DN proportionally more than the dimmer ones. This hypothesis, however, is hard to test on this database since there is already considerable saturation over the big cities.
- 3) The overall *brightness* of small settlements decreased, so that the relative share of luminosity taken by the bright lit agglomerations increased, driving the Gini coefficient up.

Of course all these scenarios can coexist and interact, and a separation of the effects is quite difficult. Other unknown economical or technological factors could also play a role. Nevertheless, we will try to test them in the next chapter.

```
% Function to plot the light Lorenz curve of a selection of countries
% INPUTS    input      : DBF histogram file from ArcGIS
%           selection  : List of countries to display (CountryIDs)
%           xmin       : First row of values to consider (DN threshold)

function lorenz_curve_dbf(input, selection, xmin)

quant = 1;                      % draw curve by 1% steps
steps = 100/quant+1;

% First row of x_values (xmin = 1 --> discard first row)
if nargin<3
    xmin = 1;
end

% Read the input (exported from ArcGIS Zonal Histogram into DBF)
[n,t] = xlsread(input);
% Read the country names (stored separately)
[nothing,names] = xlsread('country_names2.xls');

% The first column contains the x_values of the histogram
x_values = str2double(t(2:end,1));
% Where to start (xmin = threshold)
temp = find(x_values>=xmin);
xmin_index = temp(1);
x_values = x_values(xmin_index:end);

% List of countries as OBJECT IDs
t = t(1,2:end);
t = regexp替(t,'OBJEC_','');
t = str2double(t);

% Get Data - excluding the pixels with less than xmin
n = n(xmin_index:end,:);

country_names = [];
y_values = zeros(steps,length(selection));
quantiles = zeros(steps,1);

for i=1:length(selection)

    list = n(:,find(t==selection(i)));
    total_el = sum(list);
    disp(sprintf('pixels for %s: %d', char(names(selection(i))),total_el));
    el_in_quantile = round(floor(total_el./(steps-1)));
    list = create_list_2(x_values, list);
    for j=1:steps
        if j == 1
            quantiles(j) = 0;
        elseif j == steps
            quantiles(j) = sum(list((j-2)*el_in_quantile+1:end));
        else
            quantiles(j) = sum(list((j-2)*el_in_quantile+1:(j-1)*el_in_quantile));
        end
    end
    quantiles = cumsum(quantiles)/sum(list)*100;
    y_values(:,i) = quantiles;
    country_names = [country_names {sprintf('%s - Gini: %0.2f, area: %0.4fk',char(names(selection(i))),gini_dbf(input,selection(i),xmin),total_el/1000)}];
end

% PLOT
plot(0:quant:100,y_values,'--','lineWidth',2); hold on;
plot(0:quant:100,0:quant:100,:,'color','black');
xlabel('Cumulative share of pixels from lowest to highest light emission');
ylabel('Cumulative share of light emissions');
legend([country_names 'Equality line'], 'Location', 'NorthWest');
title(sprintf('Light Lorenz Curves - Year %s, DN>=%d',input(9:12),xmin),'FontWeight','bold');
```

Figure 6.12 – MATLAB Code for plotting many Lorenz curves in the same graph. The step size, the selection of countries and the DN threshold are adjustable.

6.5 Related research and distinctions

I found only one more and recent publication that uses a variation of the Gini coefficient adapted for nighttime lights³ which, in addition, normalizes the amount of light by the population density, that is retrieved from the LandScan in form of global grid (Elvidge, et al., 2012). This indicator measures the co-distribution of light *and* people.

Two results are especially interesting: about 1.2 billion people live in areas with no detectable light, and only 13% of the world population is getting 80% of the total light.

The obtained “Night Light Development Index” (NLDI) was computed per every country and was found to be (inversely) correlated ($R^2=0.71$) with the Human Development Index (HDI)⁴.

The main difference between the NLDI and the above described light Gini is that in the NLDI, the *spatial* distribution is not considered anymore⁵: the dimension *space* is canceled out by dividing the two spatially explicit datasets:

$$\left[\frac{\text{Population}}{\text{Area}} \right] = \left[\frac{\text{Population}}{\text{Light}} \right]$$

Therefore, the NLDI doesn't say anything about how light is dispersed over the space, but rather how it is distributed among people.

³ The dataset used there is the radiance calibrated composite of 2006. No time series analysis was performed.

⁴ The HDI is a composite statistic of life expectancy, education and income indices to rank countries into four tiers of human development. It was published by the United Nations Development Program.

⁵ Or better said, it is considered only at the aggregation level used, in this case at country level.

7 Urban growth

7.1 Motivation

I searched a way to quantify the spatial growth of the largest cities and dense urbanized areas. Because of the saturation occurring over the city centers, this dataset is not suited for a quantitative evaluation of the amount of light/power emitted, but is more useful to better understand the dynamics of the spatial extension of cities.

The basic research question here is: "are urban areas growing even bigger, and at what pace?" and "in which countries cities grew the most?"

7.2 Methods

In order to isolate the cities from the rest of the composites, a threshold technique was used to produce binary images. This method has several advantages: first of all, the ambiguous measure "amount of light" is replaced by the much more convenient indicator "lit area", which is measured in square kilometers. Second, the problem of saturation over cities is avoided, since in the binary image, every pixel is either considered as 'lit' or 'non lit'.

Of course the threshold plays an important role: if we set it to 1, i.e. we ignore only the completely dark pixels, we obtain huge surfaces that extend way beyond the urbanized areas. On the other hand, if we set the threshold to 63 (saturation), only the very bright pixels over the city centers are considered, whereas all the suburbs are eliminated.

After several empirical iterations, a threshold of 30 was chosen and applied to all the composites, giving the value 1 to every pixel with DN greater than 30. Accordingly, another set was created for all the pixels below or equal to 30, but greater than zero.

For both sets, the sum of bright, respective dim lit area for every country and for every year was produced used a model analog to the one presented in figure 5.2 at page 34.

7.3 Results

First of all we want to test our intuition of section 6.4: is it true that the amount of dim pixels grew proportionally more than the brighter ones? Table 7.1 gives us the answer: globally, between 1992 and 2009, the area with $DN > 30$ grew nearly 20%, whereas the area with $DN < 30$ almost 50%. At a global scale we can therefore confirm this hypothesis.

	Change of dim lit area		Change of bright lit area	
	Absolute (km ²)	Percent	Absolute (km ²)	Percent
China	+574'609	+81.41%	+95'394	+225.76%
India	+448'852	+48.41%	+21'380	+80.95%
Brazil	+243'648	+94.19%	+21'232	+57.86
Russia	+261'858	+36.33%	-25'231	-24.85%
USA	+511'651	+81.41%	-6'316	-1.44%
World¹	+4'543'889	+48.92%	+261'530	+19.43%

Table 7.1 – Change in the lit area in the world and in selected countries from 1992 to 2009. Pixel thresholds: dim light: $1 < \text{DN} \leq 30$, bright light: $\text{DN} > 30$

Figure 7.1 shows the evolution of the area with $\text{DN} > 30$ for the four countries with the biggest absolute increase from 1992 to 2009. Three of the four BRIC countries are dominating the ranking, China outclassing the other two with an impressive absolute ($95'394 \text{ km}^2$) and relative (225%) growth. The greatest development is clearly visible in the area around Shanghai (Figure 7.3) and Shenzhen-Guangzhou (Figure 7.4).

The substantial increase of light in Egypt is due to the pronounced development of the Nile delta and in general of all the coasts along the Nile, as Figure 7.2 shows.

The evolutions of India and Brazil are instead more diffuse and not referable to single hot spots, but rather to a large set of cities growing all together.

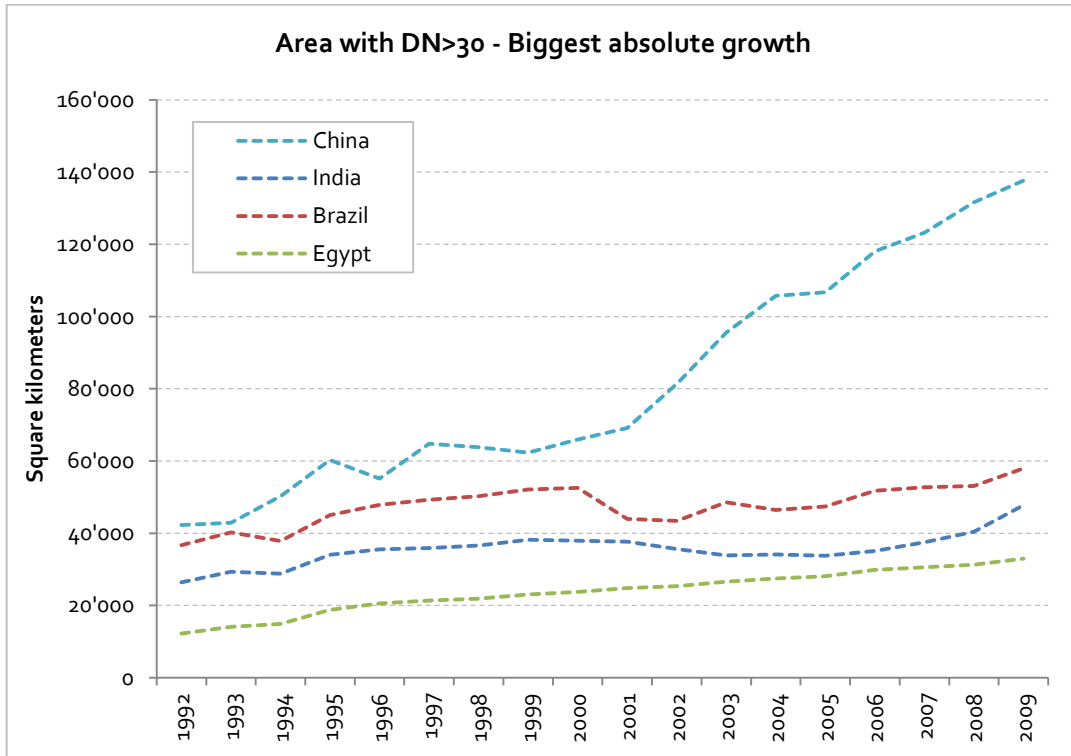


Figure 7.1 – Evolution of the area with $\text{DN} > 30$ for the countries with most absolute increase between 1992 and 2009.

¹ Countries with an area of less than 5'000 square kilometers (mainly islands) were excluded because of misleading results in the percentages. A total of 160 countries remained in the database.

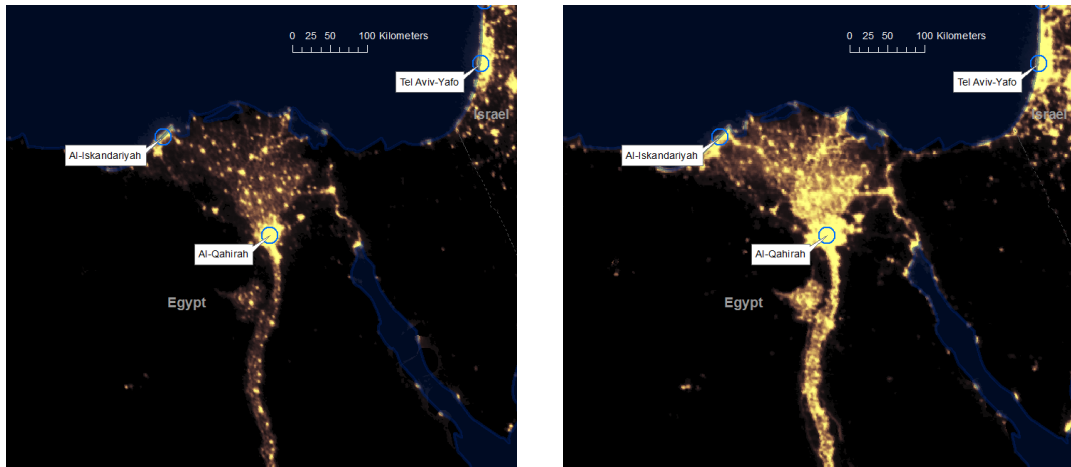


Figure 7.2 – Nile delta in 1992 (left) and 2009 (right). Nearly the totality of light emission of Egypt comes from this area and the coast of the Nile. Note the consolidations along the interconnections between the settlements.

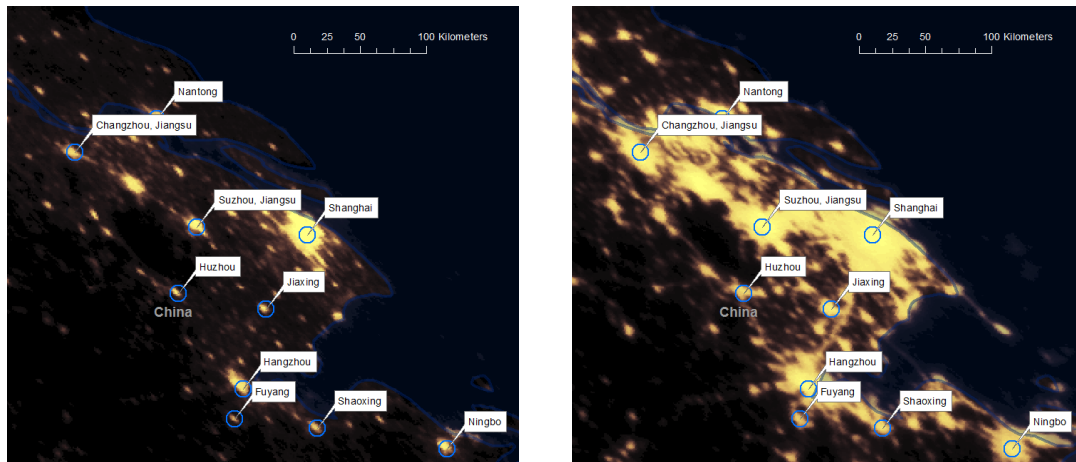


Figure 7.3 – Impressive growth of lights in China around Shanghai from 1992 (left) to 2009 (right).

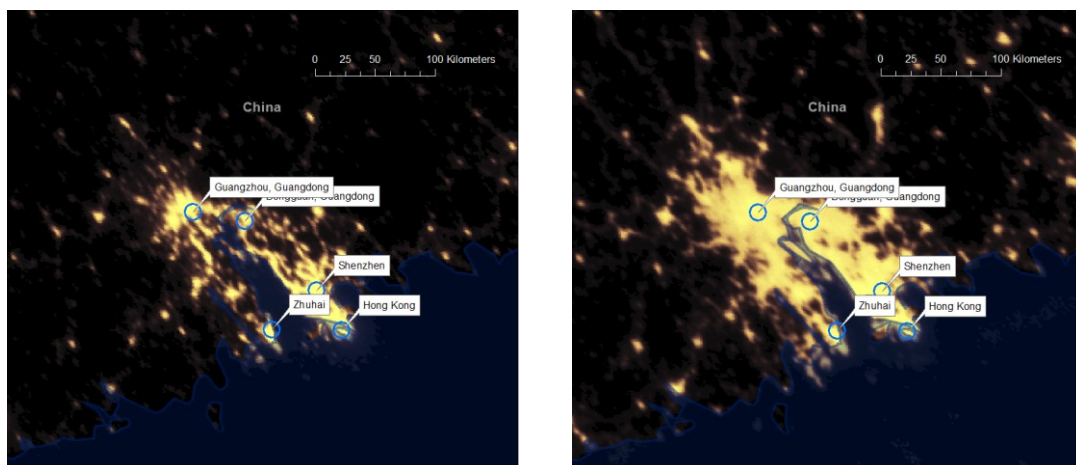


Figure 7.4 – Lights growth for the agglomeration of Shenzhen-Guangzhou from 1992 (left) to 2009 (right).

Country	1992	2009	Diff	%	Country	1992	2009	Diff	%
China	42'255	137'649	+95'394	+226%	Nigeria	2'978	3'173	+195	+7%
India	26'411	47'791	+21'380	+81%	Laos	60	239	+179	+298%
Brazil	36'694	57'926	+21'232	+58%	Macedonia	250	422	+172	+69%
Egypt	12'231	32'973	+20'742	+170%	Ethiopia	151	301	+150	+99%
Italy	41'167	57'662	+16'495	+40%	Iraq	4'531	4'680	+149	+3%
Iran	16'085	30'700	+14'615	+91%	Nicaragua	295	441	+146	+49%
Spain	25'768	40'191	+14'423	+56%	Burkina Faso	118	256	+138	+117%
Saudi Arabia	20'230	31'901	+11'671	+58%	Botswana	158	295	+137	+87%
South Korea	9'173	20'389	+11'216	+122%	Armenia	204	338	+134	+66%
Mexico	25'726	34'750	+9'024	+35%	Mali	121	254	+133	+110%
Argentina	11'607	19'906	+8'299	+71%	Bulgaria	1'213	1'339	+126	+10%
Thailand	5'320	12'682	+7'362	+138%	Benin	86	194	+108	+126%
Malaysia	3'120	10'422	+7'302	+234%	Costa Rica	923	1'027	+104	+11%
Portugal	4'208	10'709	+6'501	+154%	Kosovo	90	194	+104	+116%
France	35'514	41'569	+6'055	+17%	Zambia	592	695	+103	+17%
Poland	9'978	15'713	+5'735	+57%	Malawi	186	285	+99	+53%
United Arab Emirates	4'767	9'657	+4'890	+103%	Montenegro	87	180	+93	+107%
Turkey	6'896	11'617	+4'721	+68%	Mauritania	60	150	+90	+150%
Vietnam	437	4'784	+4'367	+1'047%	Suriname	112	196	+84	+75%
Indonesia	5'214	9'152	+3'938	+76%	Uganda	97	178	+81	+84%
Libya	2'748	6'272	+3'524	+128%	Swaziland	67	142	+75	+112%
Israel	4'971	8'026	+3'055	+61%	Mongolia	245	311	+66	+27%
Oman	1'757	4'548	+2'791	+159%	Lesotho	34	92	+58	+171%
Algeria	4'296	6'934	+2'638	+61%	Namibia	235	287	+52	+22%
Chile	2'664	5'128	+2'464	+92%	Guinea	54	104	+50	+93%
Greece	2'836	5'215	+2'379	+84%	Tanzania	297	345	+48	+16%
Taiwan	6'749	8'802	+2'053	+30%	Cameroon	291	337	+46	+16%
Romania	1'334	3'287	+1'953	+146%	Gabon	169	215	+46	+27%
Croatia	651	2'420	+1'769	+272%	The Gambia	21	63	+42	+200%
Morocco	2'350	4'113	+1'763	+75%	Bahamas	221	262	+41	+19%
Jordan	1'126	2'867	+1'741	+155%	Belize	32	70	+38	+119%
Ecuador	1'606	3'230	+1'624	+101%	Haiti	68	97	+29	+43%
Peru	1'823	3'436	+1'613	+88%	Madagascar	72	98	+26	+36%
Colombia	5'769	7'303	+1'534	+27%	Chad	39	63	+24	+62%
Pakistan	8'411	9'825	+1'414	+17%	Togo	118	138	+20	+17%
Australia	12'303	13'696	+1'393	+11%	Djibouti	14	32	+18	+129%
Switzerland	4'121	5'468	+1'347	+33%	Sierra Leone	10	25	+15	+150%
Kuwait	1'180	2'411	+1'231	+104%	Guyana	34	47	+13	+38%
Syria	2'241	3'389	+1'148	+53%	Timor Leste	3	16	+13	+433%
Austria	2'439	3'568	+1'129	+46%	Niger	106	118	+12	+11%
Serbia	1'268	2'373	+1'105	+87%	Eritrea	33	41	+8	+24%
Qatar	928	2'005	+1'077	+116%	Vanuatu	9	14	+5	+56%
Venezuela	10'770	11'800	+1'030	+10%	Congo	247	249	+2	+1%
Philippines	1'464	2'480	+1'016	+69%	Fiji	26	24	-2	-8%
Angola	228	1'211	+983	+431%	Guinea-Bissau	7	0	-7	-100%
Trinidad and Tobago	639	1'620	+981	+154%	New Zealand	1'975	1'966	-9	-1%
Yemen	577	1'483	+906	+157%	Rwanda	70	61	-9	-13%
Finland	11'059	11'937	+878	+8%	Burundi	44	34	-10	-23%
Ireland	1'706	2'493	+787	+45%	Georgia	478	467	-11	-2%
Tunisia	1'918	2'613	+695	+36%	Latvia	542	525	-17	-3%
Bolivia	861	1'547	+686	+80%	Central African	33	14	-19	-58%
Lebanon	530	1'203	+673	+127%	Nepal	146	126	-20	-14%
Bosnia	11	639	+628	+5709%	North Korea	95	66	-29	-31%
Paraguay	759	1'379	+620	+83%	Kenya	467	437	-30	-6%
Sudan	920	1'508	+588	+62%	Jamaica	564	518	-46	-8%
Cuba	510	1'060	+550	+108%	Papua New	183	123	-60	-33%
South Africa	13'297	13'834	+537	+4%	Congo, DRC	557	479	-78	-14%
Hungary	2'092	2'610	+518	+25%	Lithuania	807	723	-84	-10%
Slovenia	387	893	+506	+131%	Kyrgyzstan	559	419	-140	-25%
Uruguay	957	1'438	+481	+50%	Netherlands	11'250	11'046	-204	-2%
Guatemala	553	1'014	+461	+83%	Iceland	616	397	-219	-36%
Cyprus	634	1'094	+460	+73%	Bangladesh	1'254	1'012	-242	-19%
Czech Republic	4'827	5'249	+422	+9%	Azerbaijan	1'306	1'009	-297	-23%
Turkmenistan	1'091	1'498	+407	+37%	Zimbabwe	868	494	-374	-43%
Myanmar	268	673	+405	+153%	Tajikistan	634	149	-485	-76%
Honduras	396	792	+396	+100%	Belarus	3'052	2'541	-511	-17%
Estonia	687	1'073	+386	+56%	Moldova	784	174	-610	-78%
Ghana	688	1'072	+384	+56%	Germany	34'373	33'505	-868	-3%
Mozambique	170	532	+362	+213%	Denmark	3'170	1'901	-1'269	-40%
Dominican Republic	796	1'151	+355	+45%	Slovakia	2'684	1'256	-1'428	-53%
Afghanistan	189	499	+310	+164%	Kazakhstan	6'811	5'366	-1'445	-21%
Brunei	236	546	+310	+131%	Japan	59'241	57'409	-1'832	-3%
Albania	16	291	+275	+171%	Belgium	14'195	12'166	-2'029	-14%
Panama	520	788	+268	+52%	Uzbekistan	5'603	2'606	-2'997	-53%
Sri Lanka	517	758	+241	+47%	Sweden	14'654	9'020	-5'634	-38%
Norway	7'671	7'903	+232	+3%	United States	438'324	432'008	-6'316	-1%
Senegal	186	396	+210	+113%	United Kingdom	43'746	36'220	-7'526	-17%
Cote d'Ivoire	400	605	+205	+53%	Ukraine	15'745	5'846	-9'899	-63%
El Salvador	427	632	+205	+48%	Russia	101'529	76'298	-25'231	-25%
Cambodia	33	209	+176	+533%	Canada	79'571	52'176	-27'395	-34%

Table 7.2 – Change in bright lit area (DN>30, in km²), ordered from the largest absolute increase (Diff)

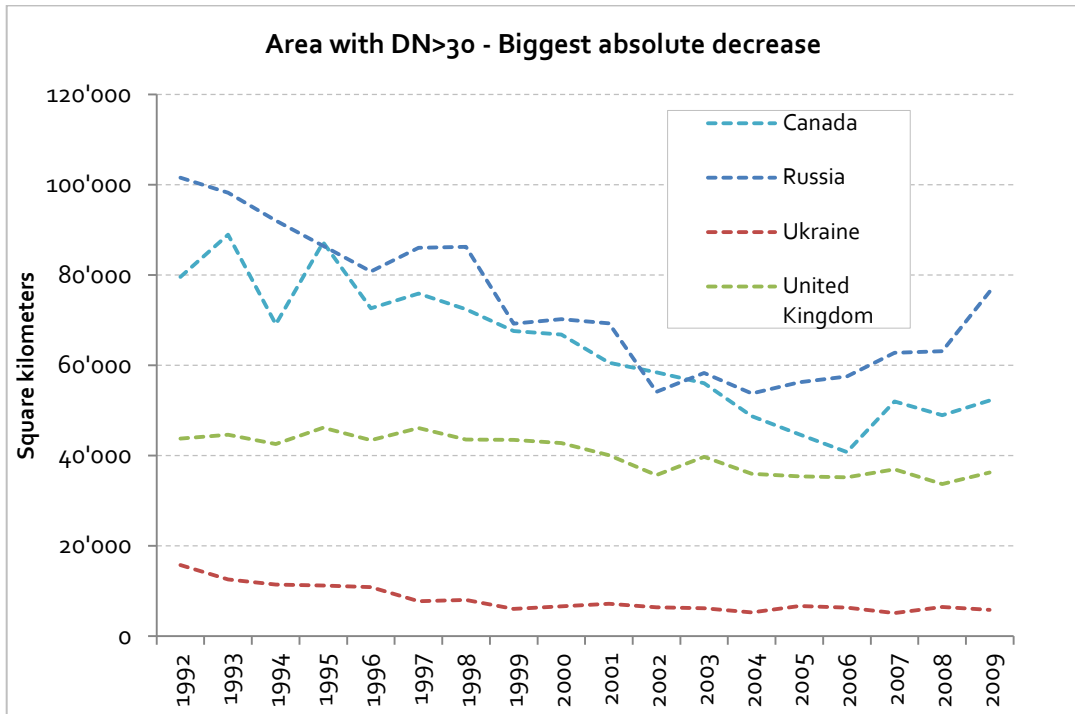


Figure 7.5 – Evolution of the area with DN>30 for the countries with largest absolute *decrease* between 1992 and 2009

Figure 7.5 shows instead the four countries with the biggest absolute *decrease* in strong lit area. Interestingly, two of them are high developed countries whereas other two are rather developing ones. Therefore, two different reasons for this decrease should coexist:

- 1) Big cities area has indeed decreased. This can again be due to different reasons such as wars, economic recession or emigration.
- 2) Light pollution in big cities has decreased. This is obviously a matter that applies to rather richer and developed countries, which can afford such projects. A clear example is Canada, where various programs were adopted from 1991 onwards to reduce the artificial sky brightness, notably from street and public lighting (Royal Astronomical Society of Canada, 2011). The worldwide reference for such programs is the International Dark-Sky association (International Dark-Sky Association, 2012).

To distinguish between the countries that had actually reduced their light pollution and those in which the urban area actually decreased, I compared the decrease in bright light with the change in urban population estimated by the indicator "Urban Population" of the World Bank (World Bank Group, 2012). The result confirms the intuition that the majority of countries showing a decrease in bright lights area performed some kind of light pollution abatement, whereas only a few countries experience an actual reduction of urban population (see table 7.3).

Another possible way to compare countries according to the extent of their bright/dim areas is to look at a simple categorization suggested in table 7.4. The great majority of countries (118, or 74%) fall in the category 1, i.e. both bright lit areas and dim lit areas increased. Only in a small fraction of countries both areas decreased or only bright light increased. A considerable amount of countries (31, i.e. 19%) instead present a pattern where bright light decreased, whereas dim light increased.

	Bright area change		Urban Population change	
	Absolute (km ²)	%	Absolute (people)	%
Russia	-25'231	-24.85%	-5'842'556	-5.35%
Ukraine	-9'899	-62.87%	-3'543'432	-10.16%
Moldova	-610	-77.81%	-249'382	-14.43%
Lithuania	-84	-10.41%	-256'730	-10.28%
Latvia	-17	-3.14%	-269'613	-14.92%
Georgia	-11	-2.30%	-332'121	-12.48%

Table 7.3 – List of countries where the decrease of bright lit areas between 1992 and 2009 coincided with a sensible reduction of the urban population. They represent only 16% of the countries with decreased bright lit area but 43% of the countries with decreased urban population. Urban population figures are estimates from the World Bank (World Bank Group, 2012).

Change between 1992 and 2009	Bright lights increased	Bright lights decreased
Dim lights increased	1 74% of countries	2 19% of countries
Dim lights decreased	3 3% of countries	4 4% of countries

Table 7.4 – Categorization of countries according to the increase, resp. decrease of bright and dim lit areas

2	3	4
Azerbaijan Bangladesh Belgium Burundi Canada Congo Denmark Fiji Georgia Germany Guinea-Bissau Iceland Jamaica Japan Kazakhstan Kenya Kyrgyzstan Latvia Lithuania Nepal Netherlands New Zealand North Korea Papua New Guinea Russia Rwanda Sweden United Kingdom United States Uzbekistan	Cambodia Israel Myanmar South Korea United Arab Emirates	Belarus Moldova Slovakia Tajikistan Ukraine Zimbabwe

Table 7.5 – List of countries which don't fall in the first category (increase of both bright and dim lights).

7.4 Agglomeration size

Let's now look at the size of single agglomerations instead of whole countries. The goal is to identify the largest, respectively the most rapidly growing conurbations. But how to isolate such entities? The official administrative boundaries are not always meaningful since big agglomerations can span across more municipalities, regions and even countries.

Therefore I used the same thresholding method described in section 7.2 and applied a segmentation function that identifies the size of each contiguous cluster. Again, the chosen threshold plays an important role, but some agglomerations are so dense and bright lit that their ranking remain consistent across multiple thresholds (see table 7.6).

First of all I plotted the rank-size distribution of the found light agglomerations, finding a clear hint for a power law: the cities are almost perfectly aligned on straight line in the log-log plot across 3 orders of magnitude (Figure 7.6). This is yet another confirmation that the size of cities follows a power law. For an extensive study on this subject, including maximum likelihood fits for the estimation of the Zipf exponent, see (Small, et al., 2010) and (Small & Elvidge, 2012). Using lower thresholds, the authors obtained an exponent of -1.00 consistent at a global and continental scale.

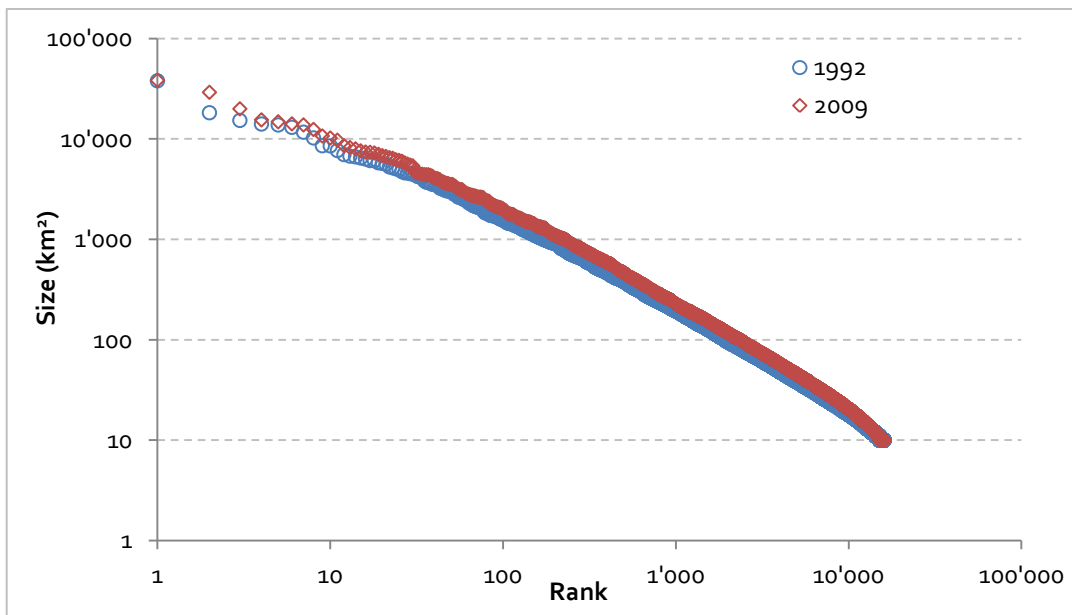


Figure 7.6 – Log-log plot of the rank-size distribution of the light agglomerations worldwide with an area greater than 10 square kilometers (threshold: DN>30). Note how the distribution for 2009 lays slightly above the one of 1992, indicating that the average size of agglomerations increased.

The second investigation, i.e. finding the agglomerations that grew the most, is less straight-forward since it required visual inspection of all the biggest clusters in order to assign them to a city. I decided to name them after the included city with the largest population size. The findings are quite interesting: while most large agglomerations of developed countries actually *decreased* their lit area, some cities in the developing countries experienced an extraordinary growth (Figure 7.7) and considerably transformed the ranking of the largest conurbations worldwide (Table 7.6).

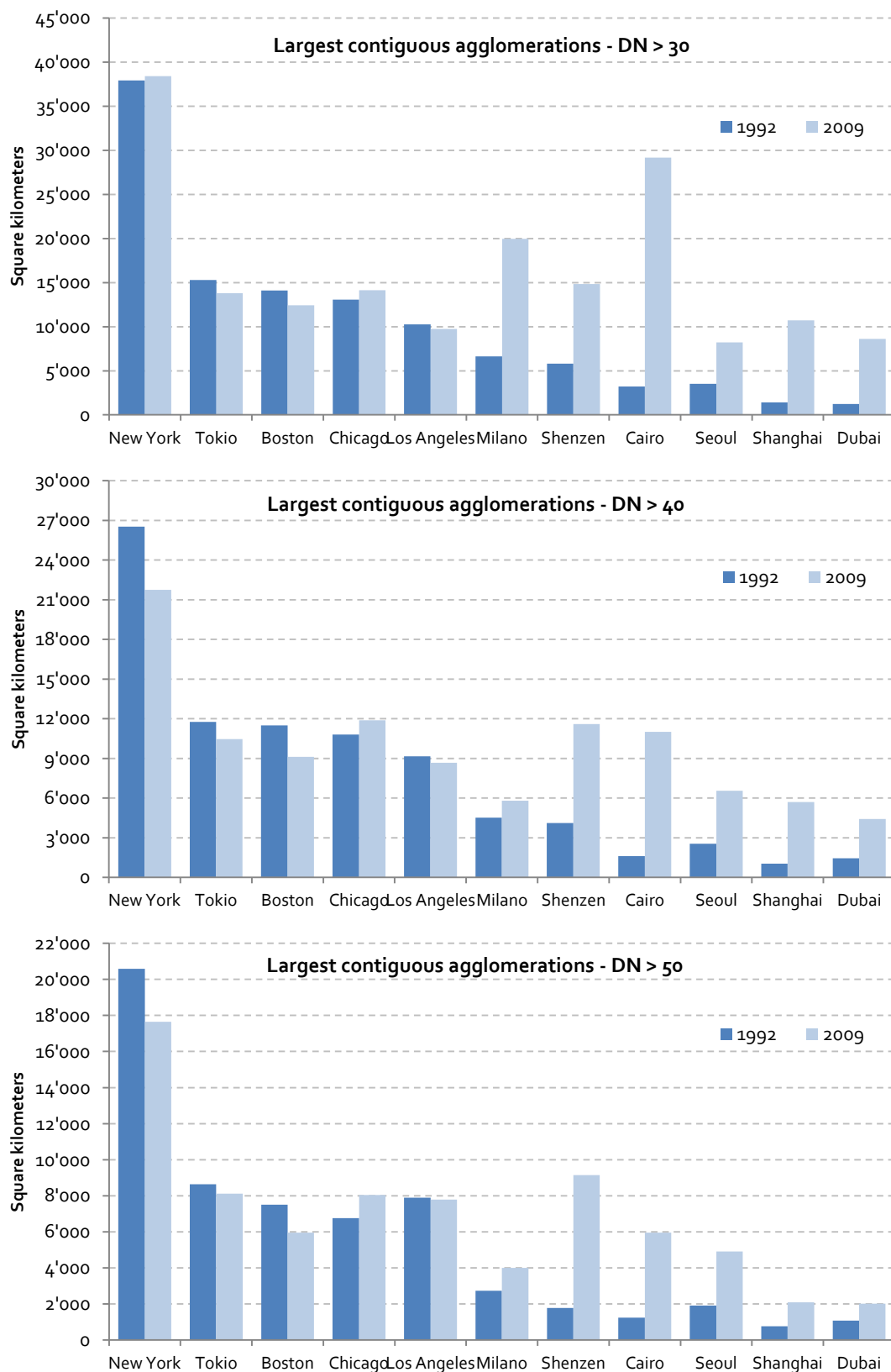


Figure 7.7 – Largest contiguous light agglomerations detected with increasing thresholds: 30 (upper), 40 (middle) and 50 (bottom). The first half of the cities shows a stable or slightly decreasing trend, whereas the other half experienced an incredible growth. Note also how the development trends are rather independent from the chosen threshold. Interesting is the remarkable growth of Cairo, due to the extraordinary development of the Nile Delta (see figure 7.2), and of the agglomeration of Milano, resulting from the coalescence with the surrounding Monza, Bergamo and Brescia.

The 20 largest contiguous light agglomerations worldwide

1992

DN > 30		DN > 40		DN > 50	
Area (km ²)	City	Area (km ²)	City	Area (km ²)	City
37'940	New York	26'533	New York	20'584	New York
18'263	Brussels	11'753	Tokyo	8'640	Tokyo
15'310	Tokyo	11'495	Boston	7'895	Los Angeles
14'101	Boston	10'812	Chicago	7'514	Boston
13'791	Liverpool	10'738	Brussels	6'761	Chicago
13'069	Chicago	9'159	Toronto	5'599	Washington
11'691	Toronto	7'452	Washington	4'588	Nagoya
10'249	Los Angeles	6'895	London	4'513	Dallas
8'568	Washington	6'231	Nagoya	4'419	London
8'541	London	5'834	Dallas	4'266	Houston
7'680	Nagoya	5'455	Houston	3'990	Osaka
6'999	Montreal	5'366	Osaka	3'882	Detroit
6'755	Osaka	5'219	Köln	3'716	Toronto
6'639	Milano	4'963	Montreal	3'700	Miami
6'473	Köln	4'860	Detroit	3'587	Cleveland
6'321	Dallas	4'745	Cleveland	3'500	San Francisco
6'098	Huston	4'533	Milano	3'464	Atlanta
6'083	Detroit	4'330	San Francisco	3'232	Montreal
5'796	Shenzhen	4'303	Tampa	3'067	Köln
5'723	Cleveland	4'238	Miami	2'920	Paris

2009

DN > 30		DN > 40		DN > 50	
Area (km ²)	City	Area (km ²)	City	Area (km ²)	City
38'418	New York	21'750	New York	17'649	New York
29'171	Cairo	11'889	Chicago	9'143	Shenzhen
19'970	Milano	11'607	Shenzhen	8'113	Tokyo
15'496	Brussels	11'016	Cairo	8'049	Chicago
14'836	Shenzhen	10'468	Tokyo	7'798	Los Angeles
14'146	Chicago	9'119	Boston	5'957	Cairo
13'810	Tokyo	8'672	Los Angeles	5'952	Boston
12'441	Boston	7'503	Tampa	5'526	Dallas
10'713	Shanghai	7'149	Brussels	5'343	Atlanta
10'225	Orlando	6'555	Seoul	5'046	Washington
9'732	Los Angeles	6'316	Washington	4'998	Houston
8'613	Dubai	6'300	Atlanta	4'912	Seoul
8'213	Seoul	6'261	Dallas	4'142	Detroit
7'978	Atlanta	5'826	Huston	4'088	Osaka
7'623	Toronto	5'799	Milano	4'004	Milano
7'415	Tel Aviv	5'709	Shanghai	3'914	Sao Paulo
7'372	Dallas	5'440	Nagoya	3'900	Nagoya
7'256	Moscow	5'201	Luxor	3'836	London
7'041	London	5'185	Detroit	3'753	Miami
6'825	Huston	5'176	London	3'518	Luxor

Table 7.6 - The 20 largest contiguous light agglomerations in 1992 (upper table) and 2009 (bottom table), with different DN thresholds. The regions were named after the included city with the largest population, but often embrace also other cities. For example, no matter with which threshold, the New York light region also includes Philadelphia, Bridgeport and Hartford. Note in particular the newcomers in 2009 from China (Shenzhen, Shanghai), Korea (Seoul), Egypt (Cairo), and Brazil (Sao Paulo).

8 Conclusions

8.1 Main findings

The global mean center of light shifted considerably to the South-East during the last two decades. This finding is consistent with similar studies done with GDP and emphasizes the fact that many countries in Asia are experiencing an extraordinary urban growth. The speed of the shift looks rather constant over the last 18 years.

In the last two decades, most countries (84%) increased their total light emission, and the worldwide total amount of luminosity increased of about 17%. This clearly indicates a substantial growth of the anthropogenic impact on the planet, from an energetic and an environmental point of view.

The relative spatial dispersion of light follows a very similar pattern in every country. The spatial light Gini coefficient measures the level of dispersion of light over the space; unexpectedly, all countries show a comparable level of statistical inequality. This suggests that the underlying dynamics of the spatial growth of human settlements could be the emerging result of universal rules, observable across very different levels of illumination and land size. For example, the spatial light Gini coefficient for the Netherlands and United States is the same (0.17, with a threshold of DN>=25), although the considered lit area differs by a factor of 35. Over the last 18 years, the Gini coefficient of most countries shows a slightly increasing trend.

Globally, dim lit area increased proportionally more than bright lit area. This finding seems contradictory to the fact that an always greater share of world population lives in cities (McKinsey Global Institute, 2012). However, the dim illuminated area could arise from suburbs surrounding current large conurbations or from new growing cities, and an eventual increase of light emitted by existing cities cannot be recorded by this dataset due to the saturation of the satellite sensors. Also, some large conurbations reduced their emissions over time.

In some developed countries, the overall amount of bright lit area and the size of the largest light agglomerations are slightly diminishing, indicating a possible reduction of light pollution. This result encourages further research in order to evaluate the success of light pollution abatement programs launched in different countries around the world.

The ranking of the largest light agglomerations worldwide is dramatically changing because of the fast-growing megalopolis in the developing countries. This phenomenon is particularly observable in China (Shenzhen, Shanghai) and Egypt (Cairo and the Nile delta). Other emerging countries like India, Brazil, Argentina, Vietnam, Indonesia also present huge growth in illumination of urban centers, although their agglomerations are not near enough to each other in order to coalesce during the thresholding operation and hence they don't appear in the 'top 20' ranking.

8.2 Selected findings from the existing literature

Nighttime lights are unquestionably a remarkable indicator of the human footprint on the planet. The amount of research that was performed in the last decade on this topic confirms this claim and provides several practical applications. The most direct and therefore reliable application is the evaluation of the worldwide light pollution.

Nighttime lights can be used to add value to the official statistics, notably GDP and GDP growth. Especially for countries with poor national income accounts, this dataset can contribute to get more reliable figures and allow assessing the economic activity at a sub-regional level. However, the relationship between economic activity and illumination is not yet fully understood and the results vary substantially for different types of countries (Henderson, et al., 2012), (Chen & Nordhaus, 2011), (Doll, et al., 2005), (Sutton, et al., 2007).

Light is a very good indicator of development and wealth. Globally, about 1.2 billion people are living in areas with no detectable light, and only 13% of the world population is getting 80% of the total light (Elvidge, et al., 2012).

Cities are the main sources of light emissions. Conurbations larger than 80km diameter account for less than 1% of all settlements but for about half the total lighted area worldwide (Small, et al., 2005).

From 2010 to 2025, the 600 fastest growing cities will account for 65% of the global GDP growth. Cities are the main drive of growth and an always bigger share of population is living in cities (McKinsey Global Institute, 2012).

8.3 Directions for future research

8.3.1 Dynamics of the urban growth

The dynamics of the spatial growth of cities could be better understood with the help of city lights in combinations with other datasets, for example road networks and traffic counts. Established models from other disciplines, like for example the percolation theory, could be used to model the temporal evolutions of urban centers as graph knots along the major transport axis. Figure 8.1 shows how large cities appear as highly connected hubs; the size of the conurbations seems to be correlated with their degree of interconnection.

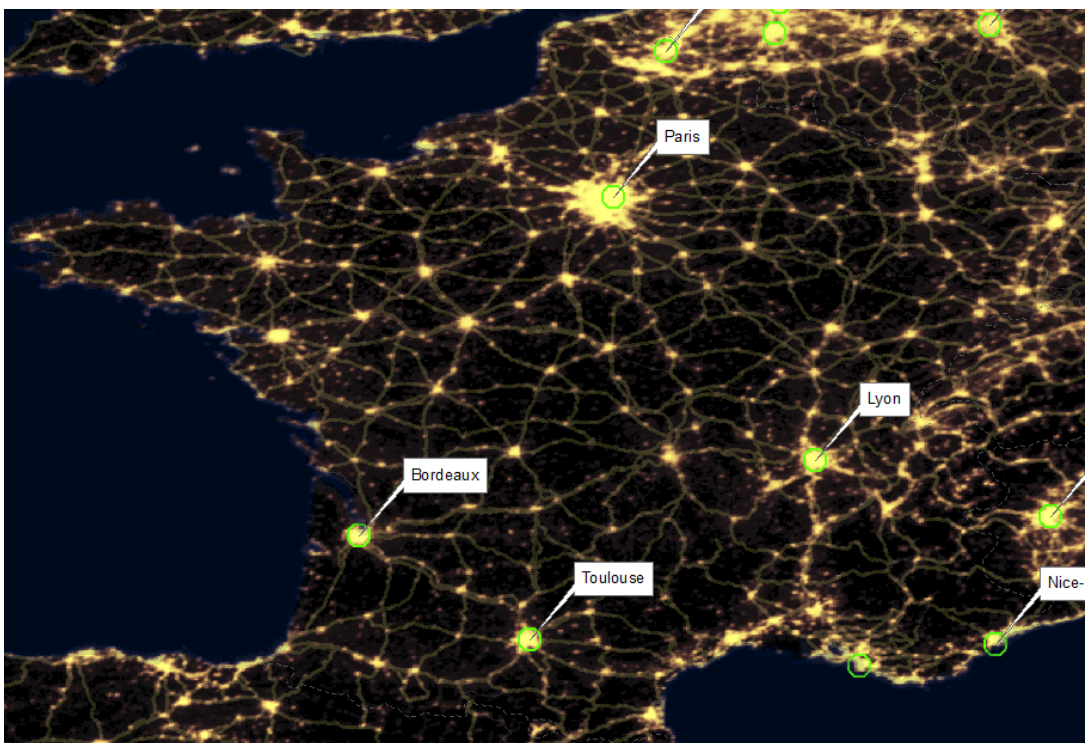


Figure 8.1 – Nighttime lights map of France for 2009, overlaid with the network of primary roads (highways). Note how the more a city is interconnected, the larger is its agglomeration size. Road network from www.esri.com.

8.3.2 Evolution of the light pollution

Some studies have been done on the light pollution worldwide and for selected countries, but there is no consistent monitoring of the temporal evolution. This dataset could help governments and NGOs to spatially plan and evaluate the effectiveness of their policies.

8.3.3 Geopolitical issues

During the visual inspection of the dataset I discovered some very interesting features that could be the base for future studies with a geopolitical motivation.

Figure 8.2 shows a portion of the land between India and Pakistan. The line indicated by the red arrow is not a river or a highway, but the fenced and floodlit border zone between these two countries, stretching over almost 3'000 km. The official purpose of the fence, surrounded by barbed wire and surveyed by soldiers, is to discourage smuggling and arms trafficking, but the relationship between the two countries is anything but relaxed, and there is no consensus on the shape of the border in the northern region of Kashmir. This dataset allows to study the progress of the fencing setup over the last two decades.



Figure 8.2 – Floodlit border between India and Pakistan in 2000.

Quite astonishing is also the almost complete darkness of North Korea. While South Korea experienced a strong increase of illumination in the last two decades, especially around the capital Seoul, North Korea doesn't emit any light, except a weak spark from the capital Pyongyang (Figure 8.3).

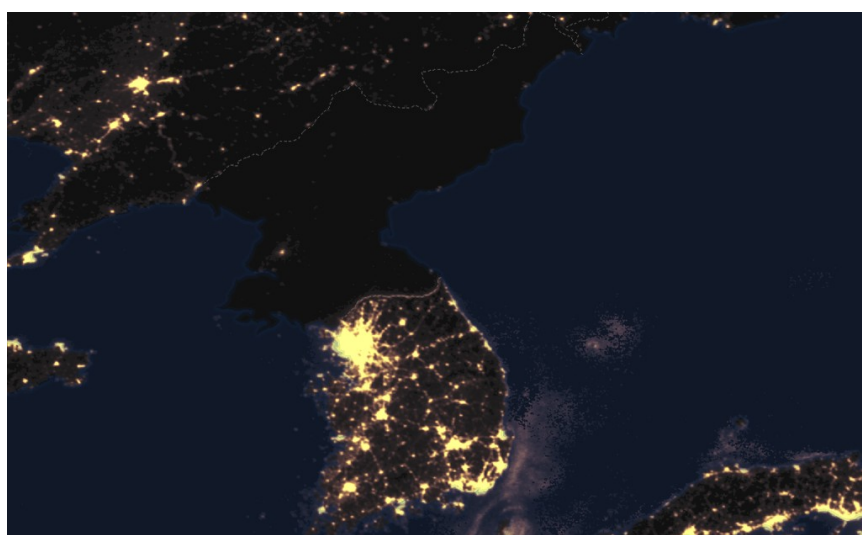


Figure 8.3 – Nighttime lights of North- and South Korea in 2009. Also here, the border between the two countries is very well visible at night.

9 List of abbreviations

APOD	Astronomy Picture Of the Day
CIESIN	Center for International Earth Science Information Network
DBF	Database File
DMSP	Defense Meteorological Satellite Program
DN	Digital Number
DoD	Department of Defense
ESRI	Environmental Systems Research Institute
GDP	Gross Domestic Product
GIS	Geographic Information System
GPW	Gridded Population of the World
HDI	Human Development Index
ISA	Impervious Surface Area
LUT	Lookup Table
NASA	National American Space Agency
NGDC	National Geophysical Data Center
NLDI	Night Light Development Index
NOAA	National Oceanic and Atmospheric Administration
NUTS	Nomenclature of Territorial Units for Statistic
OLS	Operational Linescan System
SOL	Sum of Lights
WDI	World Development Indicators

10 List of Figures and tables

Figures

- 1.1** Nighttime lights of the world
- 2.1** Visualization of a DMSP Satellite
- 2.2** Original portion of an orbit of the satellite F16 over Asia in 2009
- 2.3** Log-log plot of the DN intensity distribution of the three products for 2006
- 2.4** Log-lin histogram plot of the DN distribution in avg_x_pct and stable lights for the year 2000, F14
- 3.1** Map of world poverty based on nighttime light
- 3.2** Map of percent poverty levels for 2543 sub-national administrative units
- 3.3** City lights in the US (2009)
- 3.4** Forest fires in central Africa in 1992
- 3.5** Flaring gases from an oil platform in the North Sea
- 3.6** Onshore and offshore gas flares in Nigeria in 2009
- 3.7** Fishing boats in the sea between Japan and South Korea, in 1992
- 3.8** Artificial sky brightness at sea level in Europe
- 4.1** Stable nighttime lights map of the coast of Iran
- 4.2** Models for the join and lookup operations
- 4.3** Log-lin histogram plot of F141997, before and after the intercalibration
- 4.4** Cumulative histogram of F141997, before and after the intercalibration
- 4.5** Sum of lights for China
- 4.6** Mollweide projection of the stable lights from F101992
- 4.7** China before and after the reprojection
- 4.8** Model for averaging two satellite images of the same year
- 4.9** Sum of lights for China after averaging
- 5.1** Global center of gravity (GDP based) from year 1 to 2010, and projection for 2025
- 5.2** Model for the computation of the sum of lights at a country level for every composite
- 5.3** Model for the computation of the Mean Center
- 5.4** Light mean centers per satellite/year
- 5.5** Light mean centers per satellite
- 6.1** An example of the classical Lorenz curve
- 6.2** Model for exporting the histograms to DBF
- 6.3** MATLAB function to compute the frequencies out of the histogram amounts
- 6.4** MATLAB code to compute the Gini coefficient
- 6.5** Lorenz curves and relative Gini coefficients for selected countries in 1992
- 6.6** Lorenz curves and relative Gini coefficients for selected countries in 1992, with threshold 1
- 6.7** Lorenz curves and relative Gini coefficients for selected countries in 1992, with increasing thresholds
- 6.8** The change in the Gini coefficient for selected countries in 1992 using increasing thresholds
- 6.9** Mean and standard deviation of the Gini coefficients as function of the threshold

- 6.10** Gini coefficients for selected countries over the years, without threshold
- 6.11** Gini coefficients for selected countries with a threshold of $DN > 4$
- 6.12** MATLAB Code for plotting many Lorenz curves in the same graph
- 7.1** Evolution of the area with $DN > 30$ for the countries with most absolute increase between 1992 and 2009
- 7.2** Nile delta in 1992(left) and 2009(right)
- 7.3** Impressive growth of lights in China around Shanghai from 1992(left) to 2009 (right)
- 7.4** Lights growth from the agglomeration of Shenzhen-Guangzhou from 1992(left) to 2009(right)
- 7.5** Evolution of the area with $DN > 30$ for the countries with largest absolute decrease between 1992 and 2009
- 7.6** Log-log plot of the rank-size distribution of the light agglomerations worldwide with an area greater than 10 square kilometers
- 7.7** Largest contiguous light agglomerations detected with increasing thresholds: 30 (upper), 40 (middle) and 50 (bottom)
- 8.1** Nighttime lights map of France for 2009, overlaid with the network of primary roads (highways)
- 8.2** Floodlit border between India and Pakistan in 2000
- 8.3** Nighttime lights of North- and South Korea in 2009

Tables

- 2.1** Visualization of available composites
- 3.1** Evaluation of data and methods used in the selected publications
- 4.1** Calibration lookup table based on the coefficients of Elvidge
- 7.1** Change in the lit area in the world and in selected countries from 1992 to 2009
- 7.2** Change in bright lit area ($DN > 30$, in km²), ordered from the largest absolute increase
- 7.3** List of countries where the decrease of bright lit areas between 1992 and 2009 coincided with a sensible reduction of the urban population
- 7.4** Categorization of countries according to the increase, resp. decrease of bright and dim lit areas
- 7.5** List of countries which don't fall in the first category (increase of both bright and dim lights).
- 7.6** The 20 largest contiguous light agglomerations in 1992 (upper table) and 2009 (bottom table), with different thresholds.

Credits

All figures, tables and charts , if not explicitly specified otherwise in their caption, were created by the author, based on the freely downloadable data from (NOAA National Geophysical Data Center, 2012) and the shapefiles from (Weidmann, et al., 2010) and (Nordpil, 2009). See sections 2.2 and 4.2 for a description of these sources.

11 References

- Agnew, J., Gillespie, T., Gonzales, J. & Min, B., 2008. Baghdad nights: evaluating the US military 'surge' using nighttime light signatures. *Environment and Planning*, Volume 40, pp. 2285-2295.
- Amaral, S. et al., 2005. Estimating population and energy consumption in Brazilian Amazonia using DMSP night-time satellite data. *Computers, Environment and Urban Systems*, Volume 29, pp. 179-195.
- Amaral, S., Monteiro, V., Camara, G. & Quintanilha, J. A., 2006. DMSP/OLS night-time light imagery for urban population estimates in the Brazilian Amazon. *International Journal of Remote Sensing*, 27(5), pp. 855-870.
- Aubrecht, C. et al., 2008. A global inventory of coral reef stressors based on satellite observed nighttime lights. *Geocarto International*, 23(6), pp. 467-479.
- Baugh, K., Elvidge, C., Ghosh, T. & Ziskin, D., 2010. *Development of a 2009 Stable Lights Products using DMSP-OLS data*. Hanoi, Asia-Pacific Advanced Network.
- Bhandari, L. & Roychowdhury, K., 2011. *Night Lights and Economic Activity in India: A study using DMSP-OLS night time images*. Hanoi, Asia-Pacific Advanced Network.
- Chen, X. & Nordhaus, W., 2011. Using Luminosity data as proxy for economic statistics. *Proceedings of the National Academy of Science of the United States of America*, 108(21), pp. 8589-8594.
- Cinzano, P. & Elvidge, C., 2004. Night sky brightness at sites from DMSP-OLS satellite measurements. *Monthly Notices of the Royal Astronomical Society*, Volume 353, pp. 1107-1116.
- Cinzano, P., Falchi, F., Elvidge, C. & Baugh, K., 2000. The artificial night sky brightness mapped from DMSP satellite Operational Linescan System measurements. *Monthly Notices of the Royal Astronomical Society*, Volume 318, pp. 641-657.
- Doll, C., 2008. *CIESIN Thematic Guide to Night-time Lights Remote Sensing and its Applications*. New York: The Trustees of Columbia University.
- Doll, C., Muller, J.-P. & Morley, J., 2005. Mapping regional economic activity from night-time light satellite imagery. *Ecological Economics*, 57(2006), pp. 75-92.
- Efficient Lighting for Developing and Emerging Countries, 2012. *en.lighten*. [Online] Available at: <http://www.enlighten-initiative.org/> [Accessed 11 October 2012].
- Elvidge, C. et al., 2012. The Night Light Development Index (NLDI): a spatially explicit measure of human development from satellite data. *Social Geography*, Volume 7, pp. 23-35.
- Elvidge, C. et al., 1999. Radiance Calibration of DMSP-OLS Low-Light Imaging Data of Human Settlements. *Remote Sensing of Environment*, Volume 68, pp. 77-88.

- Elvidge, C. et al., 1997. Relation between satellite observed visible-near infrared emissions, population, economic activity and electric power consumption. *International Journal of Remote Sensing*, 18(6), pp. 1373-1379.
- Elvidge, C. et al., 2010. DMSP-OLS estimation of tropical forest area impacted by surface fires in Roraima Brazil: 1995 versus 1998. *International Journal of Remote Sensing*, 22(14), pp. 2661-2673.
- Elvidge, C. et al., 2001. Nighttime lights of the world: 1994-1995. *ISPRS Journal of Photogrammetry & Remote Sensing*, 56(2001), pp. 81-99.
- Elvidge, C. et al., 2011. National Trends in Satellite Observed Lighting: 1992-2009. *Remote Sensing*, 3(submitted for publication).
- Elvidge, C. et al., 2009. A global poverty map derived from satellite data. *Computer & Geosciences*, 35(2009), pp. 1652-1660.
- Elvidge, C. et al., 2007. Global Distribution and Density of Constructed Impervious Surfaces. *Sensors*, Volume 7, pp. 1962-1979.
- Elvidge, C. et al., 2009. A Fifteen Year Record of Global Natural Gas Flaring Derived from Satellite Data. *Energies*, 2(2009), pp. 595-622.
- Eurostat, 2012. *Regional Statistics*. [Online]
Available at:
http://epp.eurostat.ec.europa.eu/portal/page/portal/region_cities/regional_statistics/database
[Accessed 10 August 2012].
- Fuller, D. & Fulk, M., 2010. Comparison of NOAAVHRRand DMSP-OLS for operational fire monitoring in Kalimantan, Indonesia. *International Journal of Remote Sensing*, 21(1), pp. 181-187.
- Ghosh, T. et al., 2009. Estimation of Mexico's Informal Economy and Remittances Using Nighttime Imagery. *Remote Sensing*, Volume 1, pp. 418-444.
- Ghosh, T. et al., 2010. Shedding Light on the Global Distribution of Economic Activity. *Open Geography Journal*, Volume 3, pp. 147-160.
- Henderson, M., Yeh, E., Gong, P. & Elvidge, C., 2003. Validation of urban boundaries derived from global night-time satellite imagery. *International Journal of Remote Sensing*, 24(3), pp. 595-609.
- Henderson, V., Storeygard, A. & Weil, D., 2012. Measuring Economic Growth from Outer Space. *American Economic Review*, 102(2), pp. 994-1028.
- Imhoff, M. et al., 1997. Using Nighttime DMSP/OLS Images of City Lights to Estimate the Impact of Urban Land Use on Soil Resources in the United States. *Remote Sensing of Environment*, Volume 59, pp. 105-117.
- International Dark-Sky Association, 2012. *International Dark-Sky Association*. [Online]
Available at: <http://www.darksky.org/resources>
[Accessed 15 October 2012].

- Kiran Chand, T. et al., 2007. Active forest fire monitoring in Uttarakhand State, India using multi-temporal DMSP-OLS and MODIS data. *International Journal of Remote Sensing*, 28(10), pp. 2123-2132.
- Kiran Chand, T., Badarinath, K. V. S., Elvidge, C. & Tuttle, B., 2009. Spatial characterization of electrical power consumption patterns over India using temporal DMSP-OLS night-time satellite data. *International Journal of Remote Sensing*, 30(3), pp. 647-661.
- Kiyofuji, H. & Saitoh, S.-I., 2004. Use of nighttime visible images to detect Japanese common squid Todarodes pacificus fishing areas and potential migration routes in the Sea of Japan. *Marine Ecology Progress Series*, Volume 276, pp. 173-186.
- Kulkarni, R., Haynes, K., Stough, R. & Riggle, J., 2011. Revisiting Night Lights as Proxy for Economic Growth: A Multi-year light based growth indicator (LGBI) for China, India and the U.S.. *GMU School of Public Policy - Research Paper*.
- Letu, H. et al., 2010. Estimating energy consumption from night-time DMSP/OLS imagery after correction for saturation effects. *International Journal of Remote Sensing*, 31(16), pp. 4443-4458.
- Li, X. et al., 2012. Automatic intercalibration of night-time light imagery using robust regression. *Remote Sensing Letters*, 4(2013), pp. 46-55.
- Lo, C., 2001. Modeling the Population of China Using DMSP Operational Linescan System Nighttime Data. *Photogrammetric Engineering & Remote Sensing*, 67(9), pp. 1037-1047.
- Lo, C., 2002. Urban Indicators of China from Radiance-Calibrated Digital DMSP-OLS Nighttime Images. *Annals of the Association of American Geographers*, 92(2), pp. 225-240.
- Ma, T. et al., 2012. Quantitative estimation of urbanization dynamics using time series of DMSP/OLS nighttime light data: A comparative case study from China's cities. *Remote Sensing of Environment*, Volume 124, pp. 99-107.
- McKinsey Global Institute, 2012. *Urban world: Cities and the rise of the consuming class*, s.l.: McKinsey&Company.
- Min, B., 2009. *Distributing Power: Public Service Provision to the Poor in India*. Toronto, American Political Science Association Meeting.
- Newman, M., 2005. Power laws, Pareto distributions and Zipf's law. *Contemporary Physics*, 46(5), pp. 323-351.
- NOAA National Geophysical Data Center, 2012. *Version 4 DMSP-OLS Nighttime Lights Time Series*. [Online]
Available at: <http://www.ngdc.noaa.gov/dmsp/downloadV4composites.html> [Accessed 10 June 2012].
- Nordpil, 2009. *World Database of Large Urban Areas*. [Online]
Available at: <http://nordpil.com/go/resources/world-database-of-large-cities/> [Accessed 9 July 2012].

- Royal Astronomical Society of Canada, 2011. *Light-Pollution Abatement*. [Online] Available at: <http://rasc.ca/lpa> [Accessed 15 October 2012].
- Small, C. & Elvidge, C., 2012. Night on Earth: Mapping decadal changes of anthropogenic night light in Asia. *International Journal of Applied Earth Observation and Geoinformation*, Article in press(2012).
- Small, C., Elvidge, C., Balk, D. & Montgomery, M., 2010. Spatial Scaling of stable night lights. *Remote Sensing of Environment*, 115(2011), pp. 269-280.
- Small, C., Pozzi, F. & Elvidge, C., 2005. Spatial analysis of global urban extent from DMSP-OLS night lights. *Remote Sensing of Environment*, Volume 96, pp. 277-291.
- Sutton, P., 1997. Modeling Population Density with Night-Time Satellite Imagery and GIS. *Computers, Environment and Urban Systems*, 21(3/4), pp. 227-244.
- Sutton, P., Elvidge, C. & Ghosh, T., 2007. Estimation of Gross Domestic Product at Sub-National Scales using Nighttime Satellite Imagery. *International Journal of Ecological Economics & Statistics*, 8(Online), pp. 5-21.
- Sutton, P., Roberts, D., Elvidge, C. & Baugh, K., 2001. Census from Heaven: An estimate of the global human population using night-time satellite imagery. *International Journal of Remote Sensing*, 22(16), pp. 3061-3076.
- Tavoosi, H., Darvishzadeh, R., Shakiba, A. & Mirbagheri, B., 2009. *Modelling light pollution in suburbs using remote sensing and GIS*. Yokohama, The seventh International Conference on Urban Climate.
- United States Strategic Command, 2001. *U.S. Strategic Command - Satellites*. [Online] Available at: http://www.stratcom.mil/image_library/Space/21/Satellites/ [Accessed 2 October 2012].
- Weidmann, N., Kuse, D. & Skrede Gleditsch, K., 2010. The Geography of the International System: The CShapes Dataset. *International Interactions*, 36(1), pp. 86-106.
- Witmer, F. & Loughlin, J., 2011. Detecting the effects of wars in the Caucasus regions of Russia and Georgia using radiometrically normalized DMSP-OLS nighttime lights imagery. *GISciences & Remote Sensing*, Volume 4, pp. 478-500.
- World Bank Group, 2012. *The World Bank - Working for a World Free of Poverty*. [Online] Available at: www.worldbank.org [Accessed 2 November 2012].
- Zhao, N., Currit, N. & Samson, E., 2010. Net primary production and gross domestic product in China derived from satellite imagery. *Ecological Economics*, 70(2011), pp. 921-928.
- Zhuo, L. et al., 2009. Modelling the population density of China at the pixel level based on DMSP/OLS non-radiance-calibrated night-time light images. *International Journal of Remote Sensing*, 30(4), pp. 1003-1018.

